Polish J. Chem., **75**, 1603–1659 (2001)

Chemistry of Vibronic Coupling, Part 4: Off-Diagonal Vibronic Coupling Constants Across the Periodic Table

by W. Grochala and R. Hoffmann*

Department of Chemistry and Chemical Biology, Cornell University, Ithaca NY, 14853-1301 USA

(Received April 27th, 2001)

Vibronic coupling for inter–valence charge–transfer states in linear symmetric ABA molecules (A, B = s–, p– or d–block element) is investigated computationally. In particular we examine vibronic coupling as a function of the s, p, d – block nature of the A and B constituent elements. Based on density-functional theory computations for 395 triatomic molecules, we construct a map of a vibronic stability parameter **G** (defined as the ratio of asymmetric to symmetric stretching force constants) across the periodic table. Correlations of **G** *versus* the sum and difference of electronegativities of A and B elements are tested, and also vs. a useful parameter **f**, the ratio of the sum of electronegativities to an AB separation. Usually, the larger the sum of electronegativities, and the shorter the AB bond, the larger the vibronic instability. The largest vibronic instability thus occurs for interhalogen compounds. Molecules containing d-block elements exhibit trends similar to those of molecules built of p-block elements with similar electronegativities, although the latter are usually more unstable.

A molecular orbital model is developed to explain the trends obtained in our computations, as well as to build a framework for systematic manipulation of vibronic coupling constants in molecular systems. From the model we argue that vibronic coupling is usually strongest in systems built of hard Lewis acids and bases. We also show that s–p mixing and "ionic/covalent curve crossing" increase the vibronic instability of a molecule. To attain high vibronic instability, one should build a molecule of light, highly electronegative p–block elements. These findings may be of use in the experimental search for new superconducting materials.

Key words: triatomic radicals, quantum mechanical calculations, vibronic coupling, hardness, avoided crossing

There are many theories of solid-state superconductivity (SC), the best known being the BCS theory [1]. The electron-phonon coupling constant (EPCC) and the density of states at the Fermi level (DOS_F) are the most important parameters in the BCS theory. The theory predicts that the critical superconducting temperature (T_c) is high when both DOS_F and EPCC are large. Although the BCS theory cannot quantitatively explain high-temperature superconductivity, there is strong evidence of the importance of vibronic effects for the latter as well [2]. This is where our interest in vibronic

*Author to whom correspondence should be addressed, e-mail:rh34@cornell.edu

coupling constants (VCCs, the molecular analogue of the EPCCs), detailed in several preceding papers, originates. We investigate simple AB and $A_2B^{\bullet}$ molecular systems, aiming to find the relationships between the chemical nature of the elements constituting these systems and their propensity to vibronic instability. Our eventual goal is to develop a chemical strategy for tuning VCCs and EPCCs.

In our first paper we studied the behavior of VCC λ^{i}_{eg} [eV] within a broad space of three parameters: force constant (k), displacement along symmetry-breaking normal coordinate (ΔQ) and reduced oscillator mass (m) [3].

$$\lambda^{i}_{eg} = (\lambda^{i}_{eg})_v = h^{i}_{eg} \times \langle u_g|Q_i|v_e\rangle \text{ [eV]} \quad (1a) \qquad h^{i}_{eg}(Q_i) = \langle g|\delta H/\delta Q_i|e\rangle \text{ [eV/Å]} \quad (1b)$$

where g and e are the diabatic electronic wavefunctions of two vibronically coupled electronic states, u_g and v_e are vibrational wavefunctions for normal mode i, in g and e states respectively, and $\delta H/\delta Q_i$ is the derivative of Hamiltonian along the normal coordinate Q_i through which coupling occurs.

We concluded that maximizing λ^{i}_{eg} requires precise control of the nuclear geometry appropriate for a given (k, m) pair. Subsequently we concentrated on diagonal and off-diagonal linear dynamic VCCs. In a second paper we investigated the diagonal VCC (h^{i}_{ee}) for T_1 states of AB molecules where A, B = alkali metal, H or halide [4]. A parameter **f**, defined as a sum of Pauling electronegativities of the A and B elements divided by AB bond length:

$$\mathbf{f} = \mathbf{f}_{AB} = (EN_A + EN_B)/ R_{AB} \quad (2)$$

was found to be very useful in correlating h^{i}_{ee} for three distinct classes of molecules: intermetallics (M_1M_2), interhalogens (X_1X_2) and "salts" (MX), including metal hydrides (MH) and hydrogen halides (HX).

Subsequently we looked at the off-diagonal VCC (h^{i}_{eg}) for triatomic linear ABA molecules where A, B = alkali metal, H or halide [5]. We found that the same parameter **f** is of value in a qualitative description of h^{i}_{eg}: large values of **f** usually indicate large h^{i}_{eg}. We noted the utility of **f** for qualitative studies of vibronic coupling in three families of ABA molecules: intermetallic species M_2M', interhalogen species X_2X' and "salts" (M_2X and X_2M).

This paper is the fourth part in the series "Chemistry of Vibronic Coupling". We now broaden the range of molecules for which VCC's are studied [6]: we study h^{i}_{eg} for $ABA^{\bullet}$ molecules where A, B = s, p, d block element. We try to see which type of orbital (s, p, or d) helps to maximize off-diagonal VCC's in $A_2B^{\bullet}$ systems. We also explain the trends observed using a molecular orbital (MO) model.

In our next pape [7] we will try to show how the considerations of vibronic coupling constants for simple molecules may be extended to solid state systems with high-symmetry lattices.

METHODS OF CALCULATIONS

A description of the vibronic coupling model used here may be found in the *Methods of Calculations* section of [3]. Numerical data (shown in Supplement, Tables S1 and S2) have been obtained from density functional theory (DFT) B3LYP computations with a 6-311++G** basis set for light elements and LANL2DZ core potentials for heavier s- and p-block elements (for details see [4]) and for all d-block elements. An equilibrium AB bond length has been computed while constraining the ABA species to be linear. Force constants for the symmetric and antisymmetric stretching modes have been subsequently computed.

We have used the following computational packages: Gaussian'94 [8] and HyperChem 5.0 [9] for SCF and DFT calculations, YAEHMOP [10] and CACAO [11] for EH calculations.

Tables S1 and S2 may be found in the Supplementary Material to this paper.

RESULTS AND DISCUSSION

1. DFT Computations of the Off-Diagonal Vibronic Coupling Constant.

1.1. h^i_{eg} for Inter Valence Charge Transfer States of ABA Molecules where A, B = s, p – block Element.

In this section we concentrate on linear triatomic radicals of the general formula ABA$^\bullet$. Such molecules are ideal for studying the off-diagonal VCC h^i_{eg} for the antisymmetric stretching mode. This parameter is often studied with relevance to systems exhibiting a second order Jahn-Teller effect [12]. Previously we had investigated 100 linear symmetric ABA$^\bullet$ molecules [13] for A, B = H, alkali metal or halide [5]. Now we broaden this study to all s– and p–blocks of elements, investigating an additional 240 ABA$^\bullet$ molecules [14]. Numerical data for all 340 molecules are shown in Table S1 in the Supplement.

Our focus in this study is on a parameter **G**. We introduced **G** while studying vibronic coupling for ABA$^\bullet$ radicals where A, B = alkali metal, halide or H [5]; **G** is defined as ratio of force constants for the asymmetric and symmetric stretching mode:

$$\mathbf{G} = k_u/k_g \tag{3}$$

This dimensionless parameter is very useful as a quantitative description of the "asymmetric mode softening" which follows from vibronic coupling. Large positive values of **G** imply vibronic stability of a linear molecule along the asymmetric stretching coordinate (Q_{as}). Small positive values of **G** correspond to asymmetric mode softening, i.e. substantial vibronic coupling along Q_{as}. Negative **G** implies strong vibronic coupling and instability of the molecule along Q_{as}.

The electronegativity, as problematic as its definition is [15], is an obvious "chemical" parameter with which one might correlate **G**. Since the 1930's electronegativity differences have been identified with bond polarity [16], and subsequently used in diverse chemical problems (heats of formation [17], X-ray absorption edge shifts [18], XPES [19], IR [20]). Occasionally, a difference of ionization potentials has also been used [21]. On the other hand, the sum of electronegativities (which we

will use later in the paper) has been successfully applied to describe qualitatively bonding between chemical elements in solid state in the Arkel-Ketlaar diagrams [22], and to evaluate the total inductive effect of the substituents on a carbon or tin atom [23]. Parr and Pearson, using density functional theory, first introduced hardness, a parameter closely related to electronegativity [24]. Differences of hardnesses have been successfully used to derive bond energies [25], and to classify binary octet compounds [26]. On the other hand, the sum of hardnesses has been applied to construct phase diagrams in solid state [27]. Our contribution is the recognition of the utility of the parameter **f** (the sum of electronegativities divided by distance) for quantitative correlations [28]. As far as we know, a similar approach has been used only once in correlation between the experimental values of force constants and forces in diatomic H-containing molecules [29].

Why ABA radicals? The reason is that the asymmetrization process in such linear species contains the essential electron transport component that characterizes conductivity: $A^+–B^- + A^0 \rightarrow A–B–A \rightarrow A^0 + B^-–A^+$.

We discuss in this paper the motion of symmetric linear ABA molecules exclusively along an asymmetric stretching coordinate. Why do we constrain ABA molecules to a linear geometry, which may not necessarily correspond to the ground state of a molecule? The reason for that is that in the linear geometry there is a particularly effective and simple way to analyze coupling of the antisymmetric stretching mode with the charge-transfer process between A centers.

We need to emphasize here that, as important as some of these molecules are in their own right, we are interested neither in computing the lowest energy geometry for a given system [30], nor in providing a description of the whole potential energy surface determining dynamics of, for instance, the "S_N2" $A–B–A \rightarrow A^0 + B^-–A^+$ reaction [31]. Both tasks would require geometry optimization of a triatomic in a full space of nuclear coordinates. Our goal is something different, namely a comparison of vibronic stabilities within a certain class of species (linear symmetric radicals [32]), in the search for chemical trends and useful correlations.

In seeking such trends and correlations, we plot **G** *versus* the difference of Pauling electronegativities of B and A elements (Δ EN) constituting $ABA^\bullet$ molecule. Two kinds of such plots will be of particular importance: one emphasizes the affiliation of B to a given group of the periodic table, another to a given period. In Figs. 1 and 2 we show such plots (for periods II and V). In Figs. 3 and 4 we plot **G** *versus* ΔEN (for groups 1 and 13). To highlight the regularities, in each case some lines are sketched which connect in a schematic way (these are not fits) the points for a given element.

It appears that there are three kinds of shapes of **G** *vs* ΔEN plot, depending whether B is a typical nonmetal or a typical metal, or is intermediate between the two.

i) For B a typical nonmetal, such as F or O, the plot seems to peak at a certain Δ EN (we will call it hereafter $\Delta\ EN_{peak}$). **G** decreases steeply from $\Delta\ EN_{peak}$ toward more negative and more positive values of Δ EN. The formal borderline of Δ EN = 0 (for Δ EN < 0, B serves as the anion in an $A_2B^\bullet$ molecule, for Δ EN > 0, B serves as the cation) appears to play no important role for **G**. The position of the

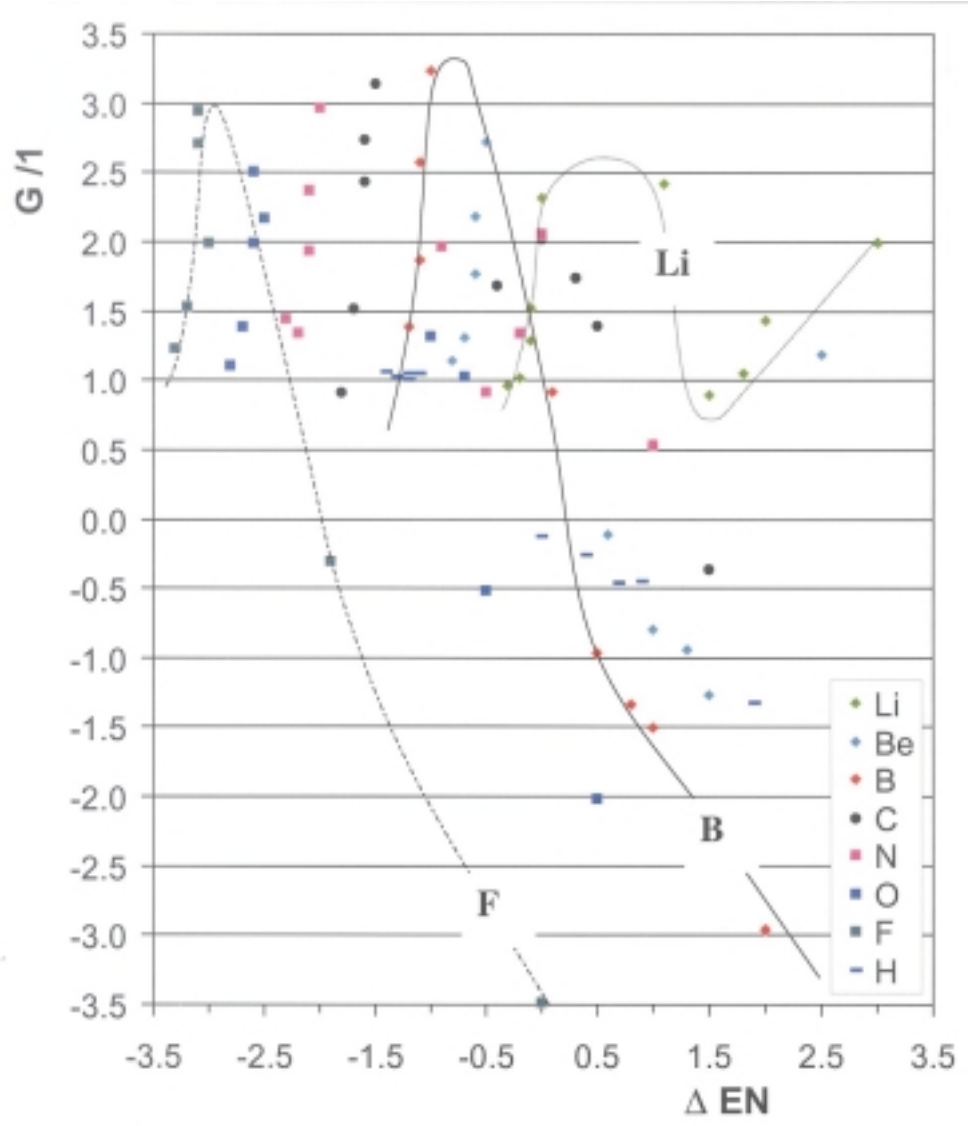

Figure 1. G for triatomic A_2B linear symmetric molecules, plotted vs difference of Pauling electronegativities of B and A elements; $\Delta EN = EN_B - EN_A$. A belongs to IInd period (data for H are also shown). Schematic lines for A= fluorine, boron, lithium (not a fit in any way) have been introduced to guide the eye.

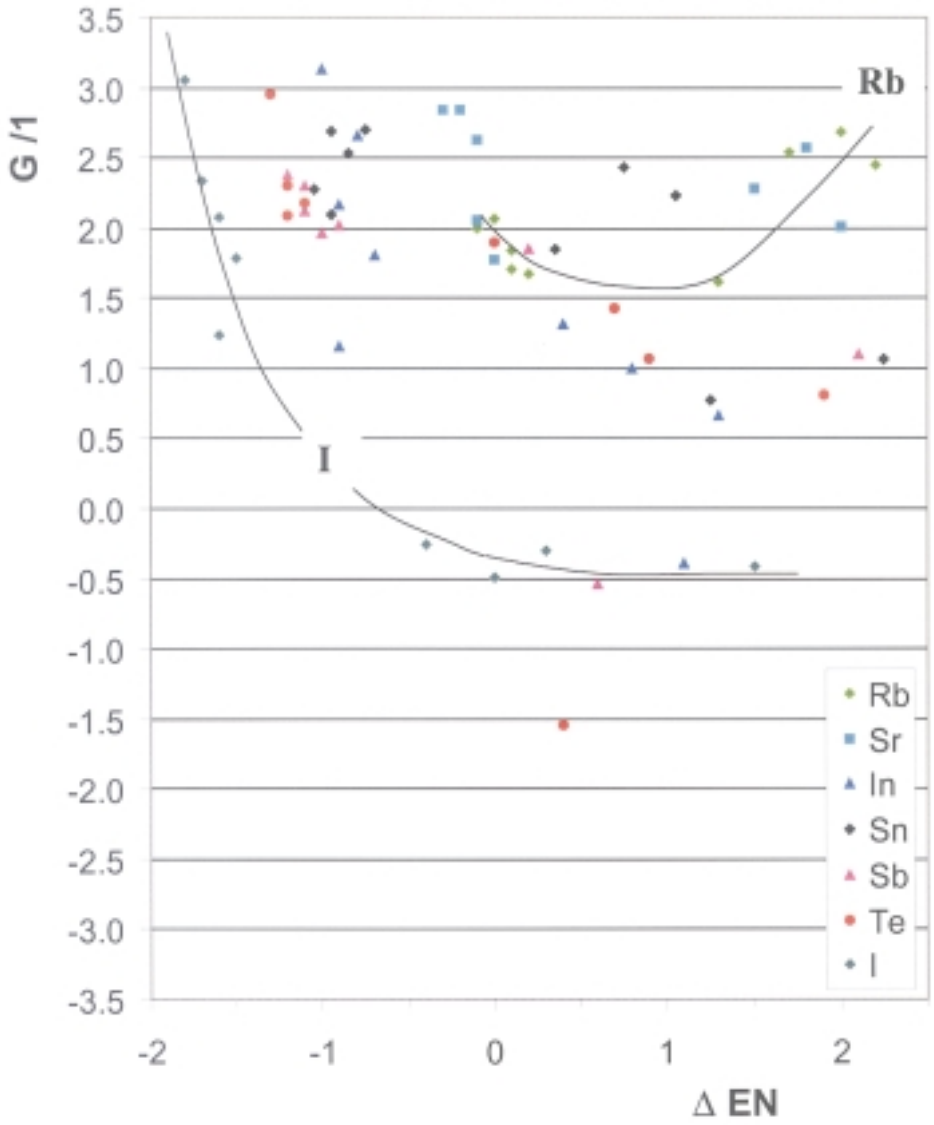

Figure 2. G for triatomic A_2B linear symmetric molecules, plotted vs difference of Pauling electronegativities of B and A elements; $\Delta EN = EN_B - EN_A$. A belongs to Vth period of the periodic table. Schematic lines for A= rubidium, iodine have been introduced to guide the eye.

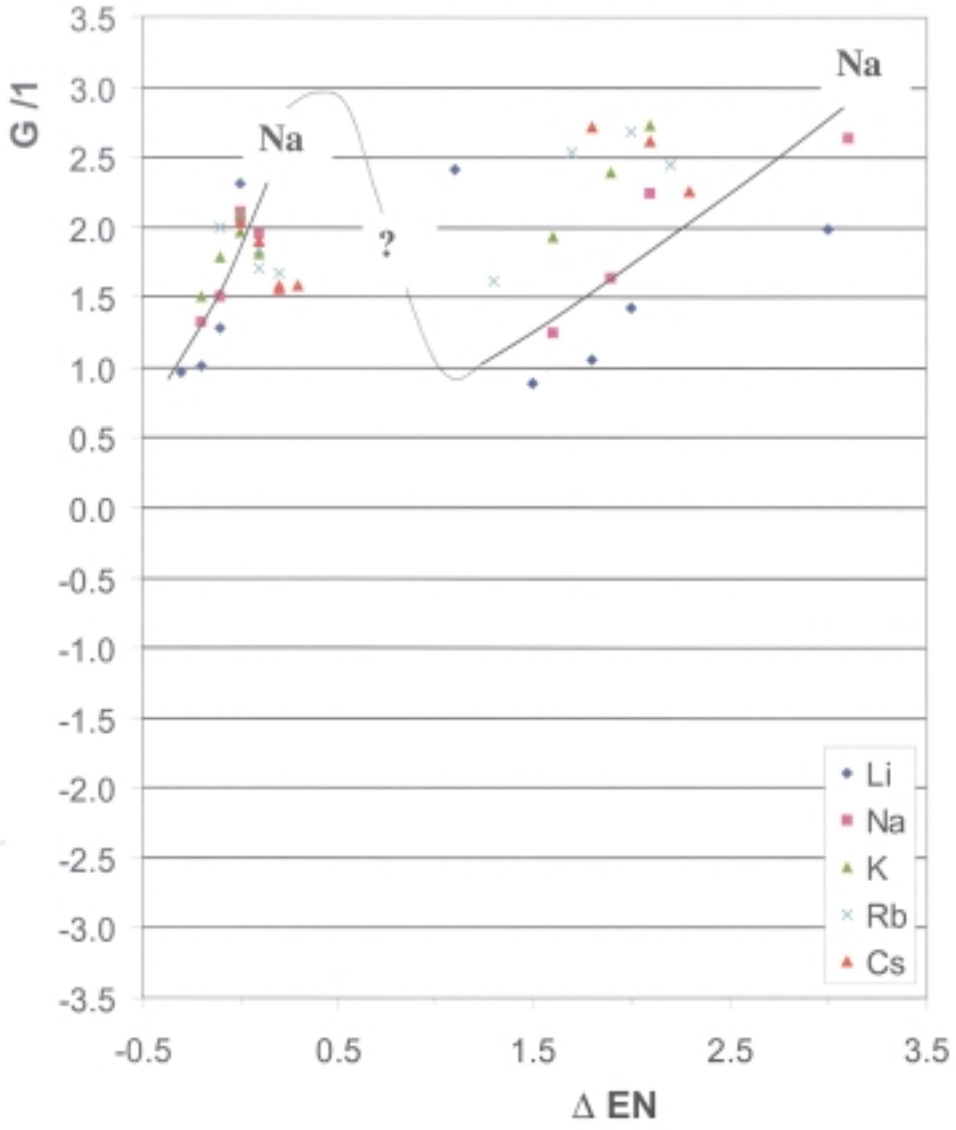

Figure 3. G for triatomic A_2B linear symmetric molecules, plotted vs difference of Pauling electronegativities of B and A elements; $\Delta EN = EN_B - EN_A$. A belongs to Ist main group of the periodic table. Schematic lines for two branches of points for A= sodium have been introduced as a guide.

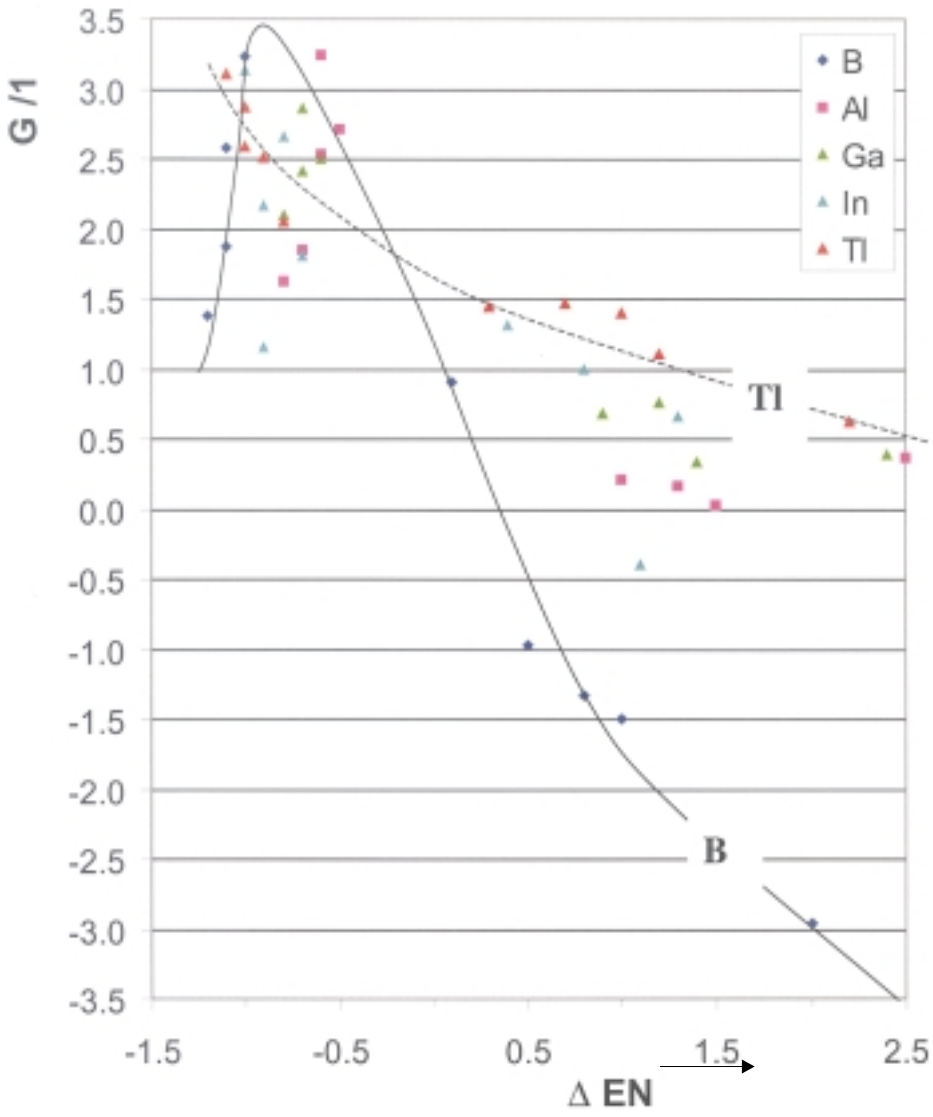

Figure 4. G for triatomic A_2B linear symmetric molecules, plotted vs difference of Pauling electronegativities of B and A elements; $\Delta EN = EN_B - EN_A$. A belongs to IIIrd main group of the periodic table. Schematic lines for A= thallium, boron have been introduced as a guide.

ΔEN_{peak} usually occurs for $\Delta EN < 0$, but is characteristic for a particular element B.

ii) The second type of plot is for B a typical metal such as Li or K. Its shape is complicated. It is composed of two branches of points: one for intermetallic A_2B molecules (near $\Delta EN = 0$) and another one for "salts" (at large positive values of ΔEN). **G** usually increases as a function of ΔEN within the second branch. It seems difficult to define a transition between the two branches.

iii) The third type of plot is found for B a semimetal (such as Sb) or a poor metal (such as Tl). It is characterized by a less steep decrease of **G** *vs* ΔEN dependence than for nonmetals. The shape of the **G** *vs* ΔEN plot seems to be intermediate between the metal- and nonmetal-type plots. It is exemplified by the right part of the plot for I, and by the left part for Rb (Fig. 2). As may be seen from Fig. 4, the transition between a metal- to semimetal- and nonmetal-type dependence is smooth, as exemplified by triatomics containing group IIIA elements.

We have observed similar features studying plots (not presented here) for elements from all other groups and periods of periodic table.

In an attempt to visualize better the dependence of the vibronic stability parameter **G** on the chemical nature of A and B elements, we construct a map of **G** within the periodic table. This is a complicated map, so in Fig. 5 we show first a "guide" to this map; it is useful in defining some of the regions. The ordinate is the difference of Pauling electronegativities of A and B elements constituting the A_2B molecule (ΔEN). The abscissa is the sum of Pauling electronegativities of B and A elements ($EN_A + EN_B$). "Ionic" molecules may be found at left and right of the diagram. "Covalent" molecules are found in the middle of the diagram. Cs_3, F_3, Cs_2F and CsF_2 molecules determine the corners of the diagram. The plot is divided roughly into four areas: "intermetallic" (s,s,s) molecules, "salt-like" (s,p,s) and (p,s,p) molecules and (p,p,p) molecules built of nonmetals. The black dot represents a homonuclear A_3 molecule. Orange solid lines indicate the position of possible A_2B and AB_2 molecules where A formally serves as anion. A_2B and AB_2 molecules, where A formally serves as cation, are found along the orange dotted lines. The labels "ionic" and "covalent" refer not to molecules in a given square, but to a rough region where $|\Delta EN|$ is large and small, respectively.

G behaves in a very interesting way, as Fig. 6, the actual map, shows. Salt-like and intermetallic molecules are vibronically stable ($\mathbf{G} \approx 2$). Molecules built of nonmetals are vibronically unstable ($\mathbf{G} < 0$). There is a formal borderline between vibronic stability and instability (the isoline $\mathbf{G} = 0$). The isoline for $\mathbf{G} = 1$ (indication of substantial asymmetric mode softening) is readily visible in Fig. 6. The transition between $\mathbf{G} = 1$ and $\mathbf{G} = 0$ regions is relatively steep, indicating that tuning of **G** might be a problem in practice.

A slight left-right asymmetry of the map presented in Fig. 6 is its interesting feature. The vibronic stability of ABA and BAB molecules is, of course, not the same. This is especially clear for molecules containing nonmetals (upper part of map in Fig. 6). Typically, the instability of BAB molecules, where B is the more electronegative ele-

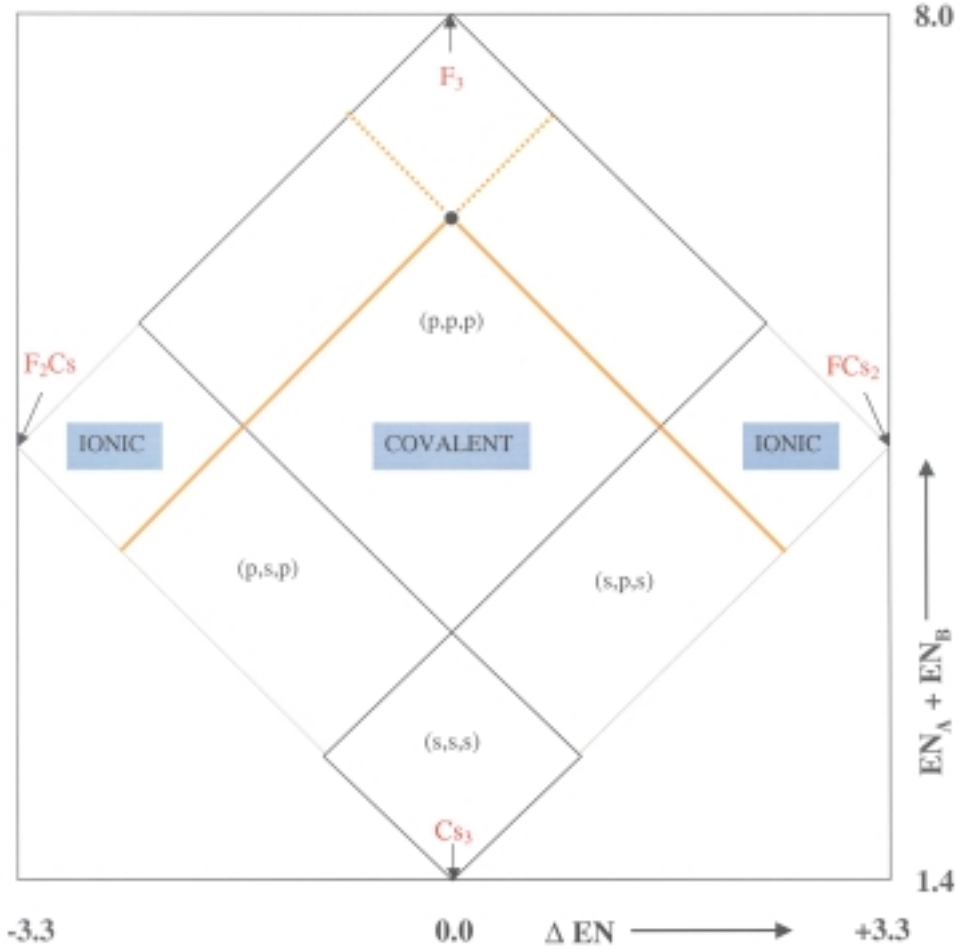

Figure 5. Schematic guide-plot for Fig.3. The ordinate is the difference of Pauling electronegativities of A and B elements constituting the A_2B molecule (Δ EN). The abscissa is the sum of Pauling electronegativities of B and A elements ($EN_A + EN_B$). "Ionic" molecules may be found at left and right of the diagram. "Covalent" molecules are found in the middle of the diagram. The labels "ionic" and "covalent" refer not to molecules in a given square, but to a rough region where |Δ EN| is large and small, respectively. Cs_3, F_3, Cs_2F and CsF_2 molecules determine the corners of the diagram. The plot is divided roughly into four areas: "intermetallic" (s,s,s) molecules, "salt-like" (s,p,s) and (p,s,p) molecules and (p,p,p) molecules built of nonmetals. The black dot represents a homonuclear A_3 molecule. Orange solid lines indicate the position of possible A_2B and AB_2 molecules, where A formally serves as anion. A_2B and AB_2 molecules, where A formally serves as cation, are found along the orange dotted lines.

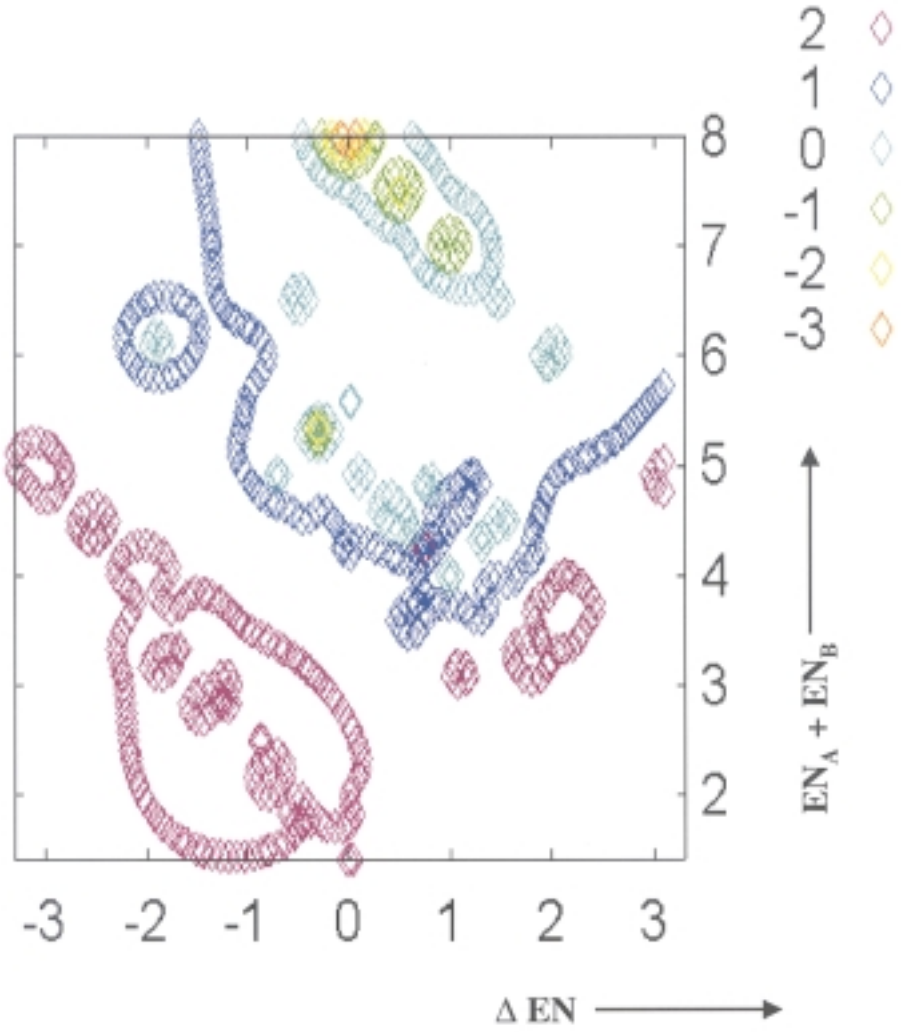

Figure 6. Map of vibronic stability parameter (**G**) in the periodic table of elements. The ordinate is Δ EN, the abscissa is ($EN_A + EN_B$). For a more detailed description see text. Fig. 5 is a guide to this plot.

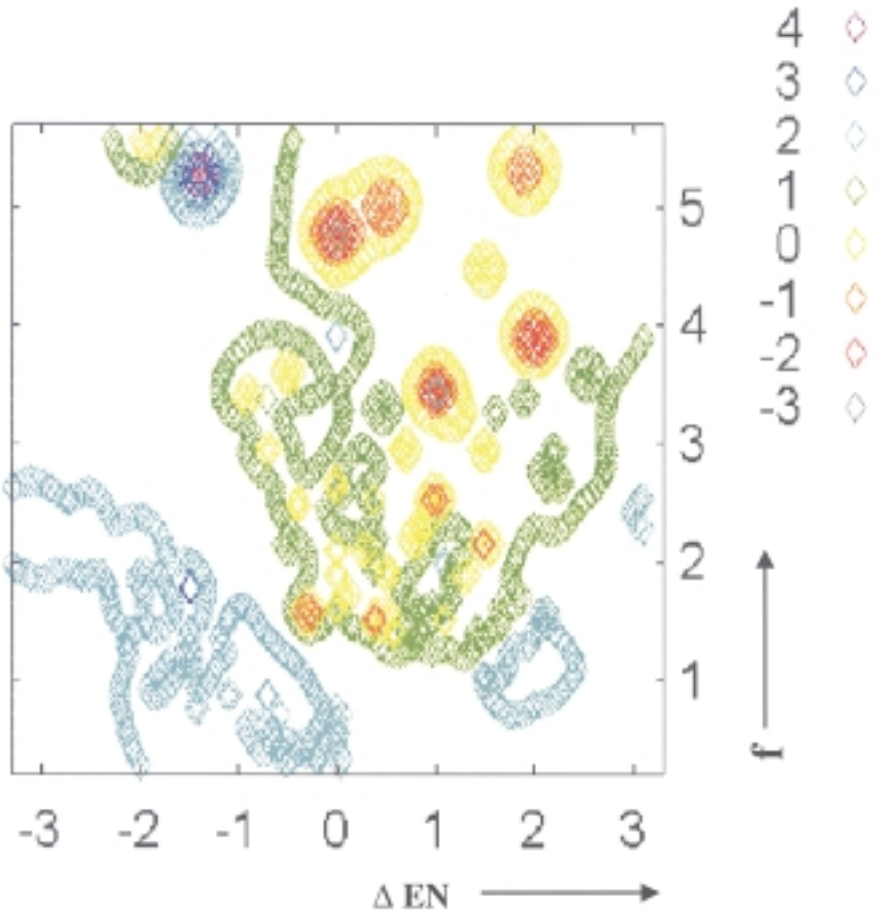

Figure 7. Map of vibronic stability parameter (**G**) in the periodic table of elements. The ordinate is Δ EN, the abscissa is **f**. For a more detailed description see text.

ment, (such as F_2H with **G** = –0.31) is smaller than that of ABA molecules (such as H_2F with **G** = –1.33) [33].

Previously we found that parameter **f** (see Eq. 2 above, **f** is the sum of the electronegativities divided by the equilibrium bond length) is of use in describing vibronic effects in AB and A_2B molecules [4,5]. Let us try then to correlate **G** with **f** (**f** substitutes ($EN_A + EN_B$) as a variable in Fig. 6). This new map is presented in Fig. 7.

Fig. 7 resembles Fig. 6 in its general shape. Molecules with large values of **f** are the most vibronically unstable species. The left-right asymmetry of the plot presented in Fig. 7 is even more evident than in Fig. 6. It is remarkable that this simple empirical parameter, **f**, again proves useful for a qualitative description of the vibronic coupling phenomenon.

The primary conclusions of this section are:

i) In looking for large vibronic instability in A_2B molecules one should search among molecules with large **f** [34]. Such species are usually built of nonmetals with short AB bonds.

ii) ABA molecules (where B is more electronegative than A) are usually more vibronically unstable than the corresponding BAB molecules.

Let us now examine vibronic coupling in triatomic linear symmetric molecules containing d-block elements as well.

1.2. h_{eg}^{i} for IVCT States of ABA Molecules where A = s, p – block Element, B = d – block Element.

The p- (C [35], Bi [36]) and especially the d-block elements (Cu [37], recently Hf [38]) are at the heart of real breakthroughs in solid-state superconductivity. We will now examine vibronic coupling in molecules containing d-block elements.

Studying molecules containing d-block elements requires assuming a certain multiplicity. For consistency, and to compare molecules containing s-, p- and d-block elements, we will limit our mixed-valence $A_2B^{\bullet}$ radicals to doublet states. Such states may or may not be the ground state of the molecule in question.

We have investigated molecules containing two distinct sets of d-block metals. One group contains Ti, Zr and Hf – the most electropositive elements in the d-block (EN_{Hf} = 1.3, compare to EN_{Mg} = 1.2). Another set contains noble and semi-noble metals (group VIIIB and IXB) – the most electronegative elements in the d-block (EN_{Au} = 2.5, compare to EN_I = 2.5). Molecules containing d-block elements would occupy a broad space in our Fig. 5.

Is there a bridge between vibronic coupling in molecules containing s- and p-block elements and those with d-block elements? May such a connection be described using such simple empirical parameters as EN or **f**? How might one distinguish between Cu, Hg, Bi, Fe, Re, whose electronegativity is nearly equal? We do *not* expect that electronegativity – although useful in so many areas of chemistry – will describe well the whole richness of so many features of different elements. Let us, however, make a try. If we used the map presented in Fig. 6 as a guide for molecules

containing d-block elements, we would conclude that most such A_2B molecules should be vibronically unstable (especially these containing noble metals). Some of these molecules might be subject only to significant asymmetric mode softening.

Let us now confront these expectations with the result of DFT computations. Fig. 8 plots the vibronic stability parameter **G** for chosen linear symmetric A_2B molecules [39] *vs*. the difference of Pauling electronegativities of A and B elements (A is a given d-block element, B is a s- or p-block element).

It is clear from Fig.8 that triatomics containing d-block elements do not behave as predicted based on trends for s- and p-block elements. All the molecules investigated are vibronically stable, contrary to our expectations [40]. There is substantial vibronic coupling (**G** < 1.5) in seven molecules: four Au-containing ones, one Ru-containing one, and two Os-containing ones. Absolute values of **G** for triatomics containing d-block elements are, however, larger than for the respective p-block elements containing molecules of similar EN.

Are not there any similarities in vibronic stability in p-block- and d-block-containing molecules? We think there are. The shape of **G** *vs*. Δ EN dependence for Au is very similar to that observed before for **I** (iodine) – it is typical of nonmetals or poor metals. On other hand, the general shape of the **G** *vs*. Δ EN dependence for Cu is more similar to that observed before for metallic s- and p-block elements. This documents that vibronic stability in molecules containing d-block elements exhibits *trends* similar to ones observed for molecules containing s- and p-block elements.

2. Model of Vibronic Coupling Along Q_{as} in Symmetric Linear $ABA^{\bullet}$ systems – MO Picture.

How to understand and predict in a qualitative way vibronic stability or instability in a large family of linear symmetric triatomics? We will try to answer this question using first a simple molecular orbital model. Two levels of theory are explored: extended Hückel theory (EH) and DFT. EH will help us establish a framework of discussion for vibronic effects. DFT will enable us to add more subtle quantitative effects to the qualitative backbone introduced by EH.

2.1. Vibronic Coupling in the Extended Hückel Model.

Simplistic thinking within EH helped us build a qualitative framework for vibronic coupling [41]. Let us use now a similar approach. We choose a linear symmetric H_3 molecule as a general model for A_3 molecules. Let us follow the normal coordinate for antisymmetric stretching ($Q = Q_{as}$) in this system and observe what happens to the MOs.

Fig. 9 shows the molecular orbitals for H_3 molecule during distortion along Q_{as}. The starting geometry has an H–H bond length of 0.931 Å (the result of a DFT optimization for a linear H_3 constrained to be symmetric). Schematic drawings illustrate the contribution of the atomic orbitals to the MOs of H_3.

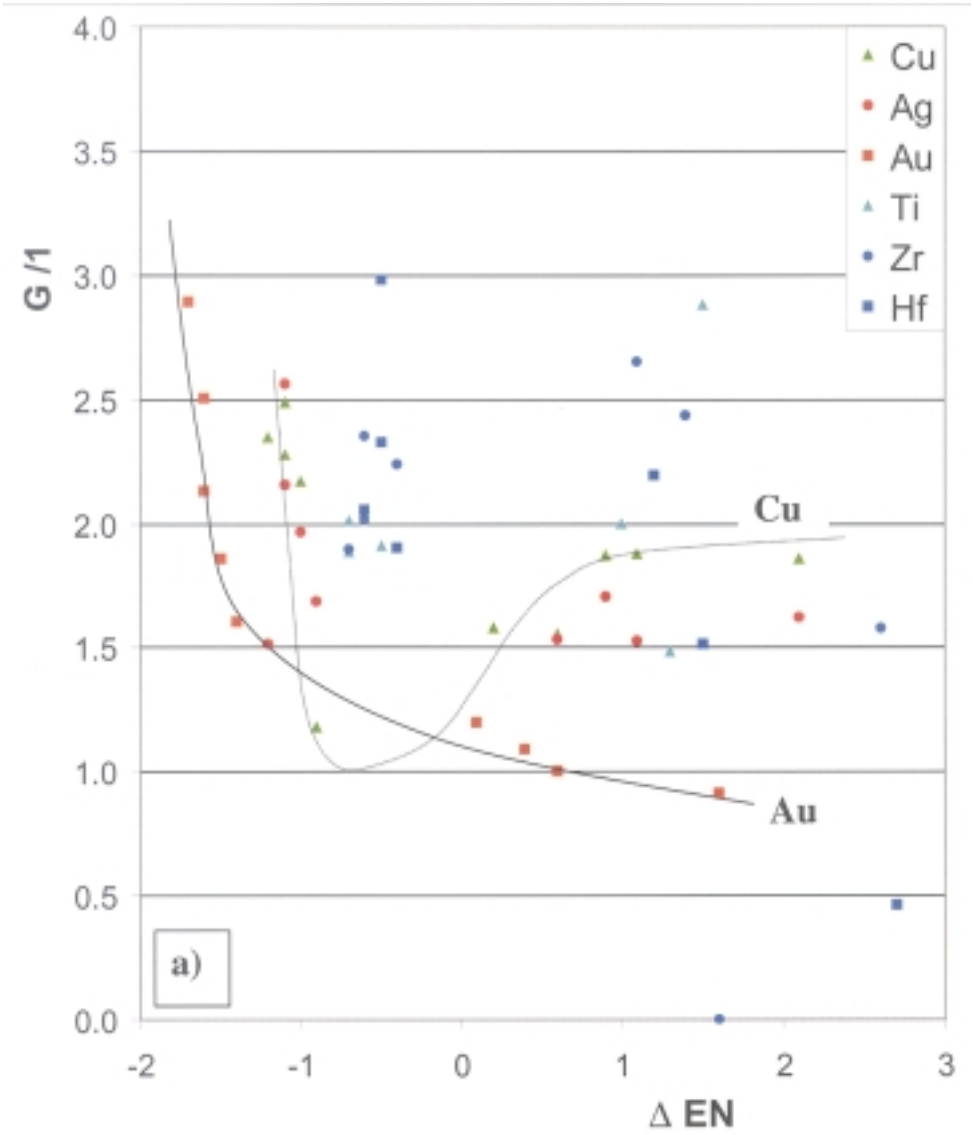

Figure 8a. Plot of vibronic stability parameter **G** for linear symmetric A_2B molecules *vs*. difference of Pauling electronegativities of B and A elements. a) A belongs to group 10 or 4. B = alkali metal, H or halogen. Arbitrarily drawn lines have been introduced to guide the eye to trends for A= Cu, Au.

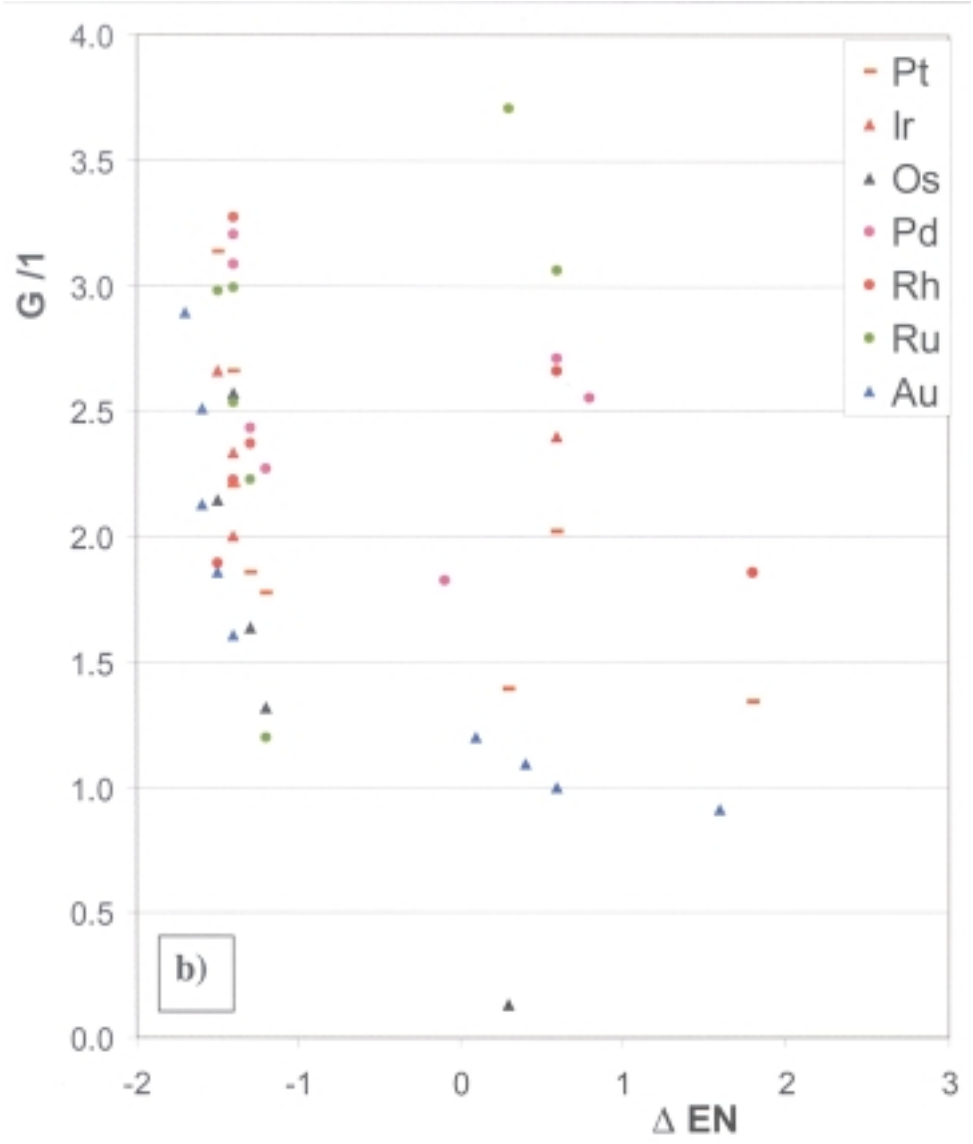

Figure 8b. Plot of vibronic stability parameter **G** for linear symmetric A_2B molecules *vs*. difference of Pauling electronegativities of B and A elements. b) A belongs to "noble metals". B = alkali metal, H or halogen.

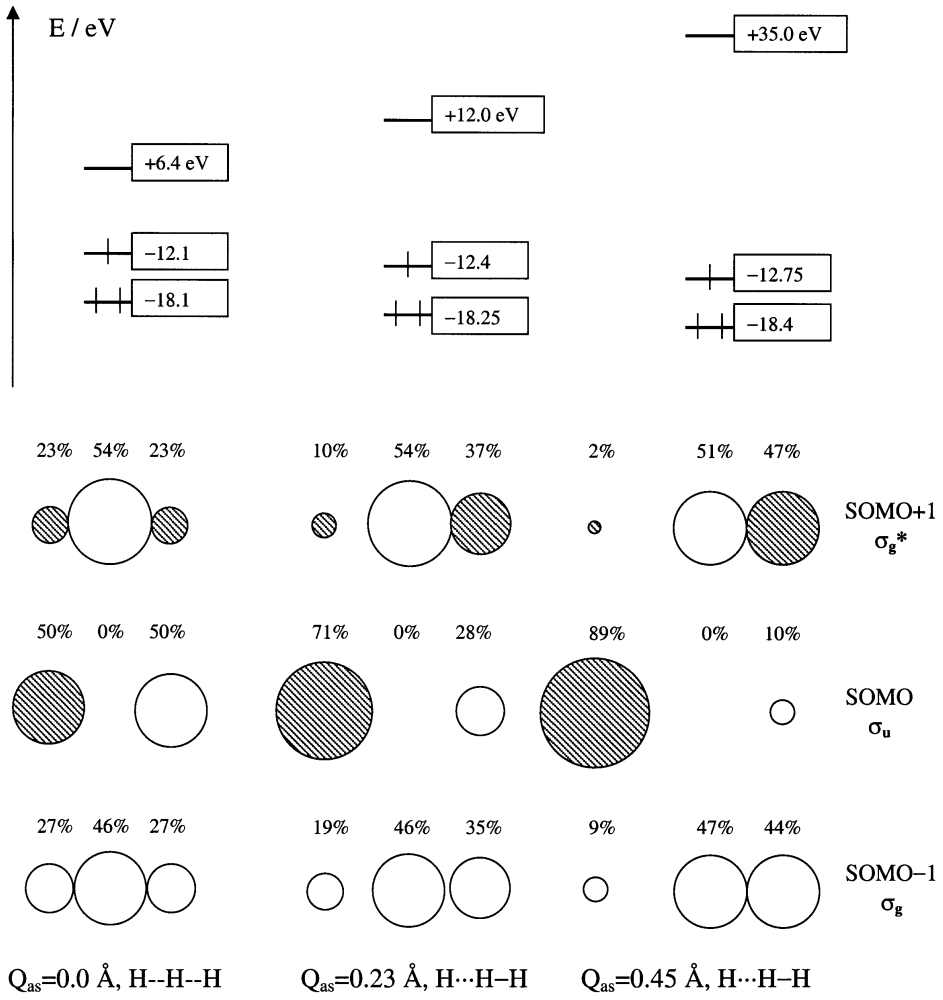

Figure 9. Following the normal coordinate for an antisymmetric stretch Q_{as} in a linear symmetric H_3 molecule (the EH computation). The sizes of the circles are a schematic indication of the AO contribution in the MO; the actual percentages are given.

The evolution of the MOs of H_3 during distortion is easily described. There are three σ MOs. In order of increasing energy these are the σ_g (SOMO-1), σ_u (SOMO) and σ^*_g (SOMO+1) of the undistorted *i.e.* symmetric molecule (SOMO is a singly occupied molecular orbital). The σ_g is nearest neighbor H–H bonding, σ_u is nonbonding and σ^*_g is antibonding. In $D_{\infty h}$ these canonical orbitals do not mix. However, as the $D_{\infty h}$ symmetry is broken in a deformation along Q_{as}, all σ orbitals may mix with one another. There is a decrease in energy connected with this distortion (for 3 electrons in the system). In the discussion that follows we use the σ_g, σ_u and σ^*_g notation for the three MO's even when the symmetry is lowered to $C_{\infty v}$ along Q_{as}.

The orbitals of a significantly asymmetric molecule are substantially different. For (exaggerated) Q_{as} = 0.45 Å the SOMO and SOMO + 1 resemble bonding and antibonding σ and σ* orbitals of an H_2 molecule and the SOMO has its main contribution from an "isolated" H atom. The result is expected; an excursion along Q_{as} brings about localization to a single strongly bound H–H molecule and an H atom.

Let us trace the perturbation of this MO scheme as we change the extended Hückel Coulomb parameter H_{ii} for the middle H atom. In this way we can simulate the substitution of the central atom by more electronegative/electropositive elements, which is what the **G** or k_u plots study. We have varied the Hückel H_{ii} for the middle H atom over broad limits (keeping the H–H separation of R_0 = 0.931 Å = const., as optimized for a symmetric linear H_3 molecule at the B3LYP/6-311++G** level).

The resulting energy levels and schematic MO pictures are presented in Fig. 10.

We show three extreme cases: the difference of Hückel parameters between central and side H atoms (ΔH_{ii} defined as H_{ii} (H′) – H_{ii} (H) in an HH′H molecule; ΔH_{ii} is used as a variable in Figs. 12, 13 and 14) being a) –15 eV, b) 0 eV and c) +15 eV. The starting point is the standard hydrogen H_{ii} of –13.6 eV. The H_{ii}'s of the terminal atoms are kept constant, only that of the central atom is varied. Cases a) and c) simulate (in exaggerated manner) the electronegativity effect of substitution in H_2F and H_2Cs molecules, respectively [42]. We will therefore denote these cases as H_2X and H_2M, respectively.

What are the basic similarities and differences between the three cases presented in Fig. 10? First, we immediately notice *no* change in the shape and energy of the SOMO (σ_u). This is obvious, considering that the perturbation is in the nodal plane of the σ_u. In a self-consistent calculation, the energy of the σ_u will actually change as the electronegativity of the perturbed ligands makes the end atoms more or less positive. Second, the ΔH_{ii} = –15 eV and ΔH_{ii} = +15 eV cases are rough "mirror images" of each other. We mean here that contributions from atomic orbitals to σ_g for ΔH_{ii} = –15 eV are close to contributions from the same atomic orbitals to σ_g^* for ΔH_{ii} = +15 eV (except for the different H-H bonding/antibonding character of both MOs). The same is true for σ_g^* at ΔH_{ii} = –15 eV and σ_g at ΔH_{ii} = +15 eV. Third, and as expected, paired orbitals (SOMO±1, *i.e.* σ_g and σ_g^*) localize, so that in the bonding MO the density is larger on the more electronegative atom, while the reverse is true in the antibonding MO [43]. As a consequence of that localization the charge distribution in "H_2X" and "H_2M" is, respectively, closer to $(H_2^{+\bullet})X^-$ and $(H_2^{-\bullet})M^+$, rather than $H_2(X^\bullet)$ and $H_2(M^\bullet)$. Fourth, as may be seen in Fig. 6b, the energy of σ_g strongly *increases* in direction $H_2X \rightarrow H_3 \rightarrow H_2M$ while the energy of σ_g^* strongly *decreases* in the same direction.

Let us take now a vibronic coupling perspective on the three cases analyzed. Using perturbation theory, one may write the expression for the perturbed wavefunction of a given *i*-th MO as:

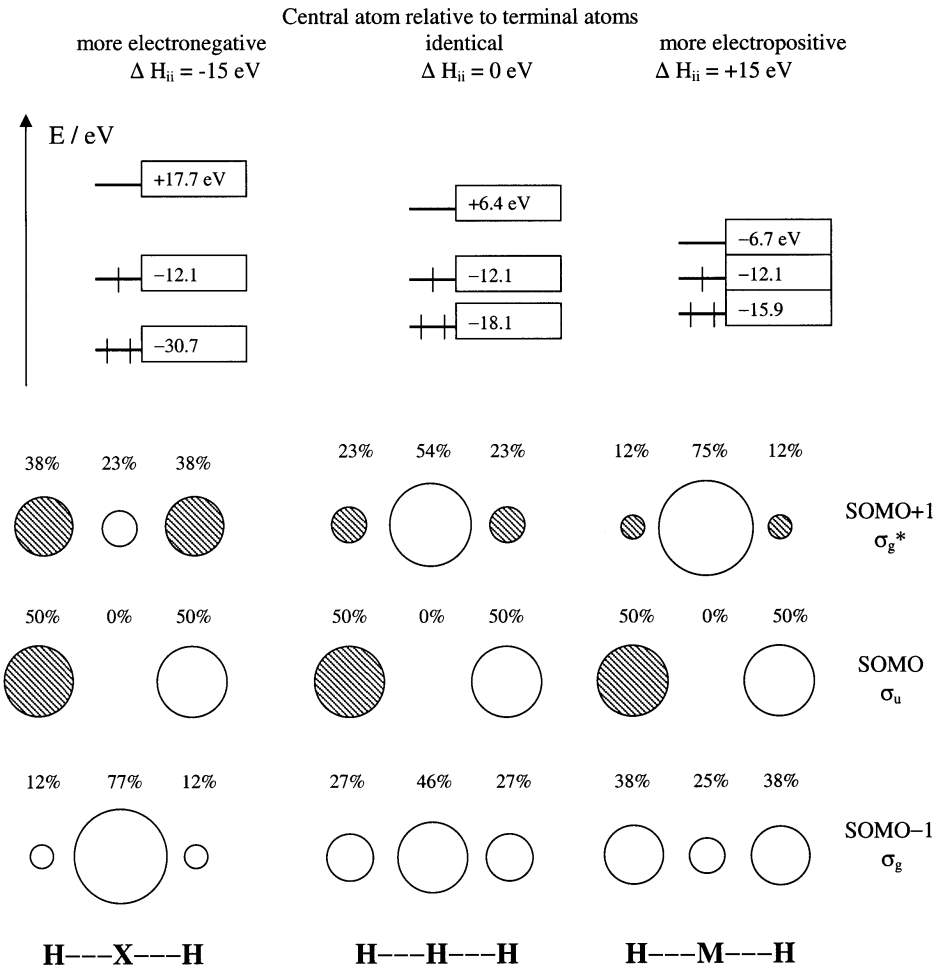

Figure 10. MO scheme for a linear symmetric AHA molecule with extended Hückel H_{ii} for central H atom varied. We show three cases (H_2X, H_3, H_2M) described in text.

$$\psi_i' = \psi_i^0 + \sum_{i \neq j} \frac{H_{ij}'}{E_i^0 - E_j^0} \psi_j^0 \tag{4}$$

where ψ_i' is the perturbed wavefunction of the *i*-th MO, ψ_i^0 is the initial wavefunction of the *i*-th MO, ψ_j^0 is the initial wavefunction of an admixing MO, E_i^0 is the energy of the initial given MO, E_j^0 is the energy of the initial admixing MO, H_{ij}' is the off-diagonal mixing element. The summation is over all MOs different than the *i*-th.

The geometry change (asymmetrization of a molecule) is the perturbation in question [44].

Given that, one would reason that the vibronic mixing along Q_{as} will be large if:

i) the energy gap between mixing orbitals ($E_i^0 - E_j^0$) is small, and

ii) the atomic contributions to given MOs are such as to maximize mixing of orbitals along Q_{as}.

For H_2M, the computed σ_g/σ_u and σ_u/σ_g^* energy gaps are about 3.8 eV and 5.4 eV, respectively. For H_2X, the respective computed gaps are about 18.6 eV and 29.8 eV. Thus, following the reasoning of i) above, one might conclude that vibronic stability would increase in the order: H_2M, H_3, H_2X. This is contrary to our DFT computations (section 1.1).

We turn then to criterion ii). To make the following discussion clearer, we will call hereafter the three hydrogen atoms in the H–H–H molecule of Figs. 9 and 10 H_{left}, H_{center} and H_{right}, respectively. Let us look again at Figs. 9 and 10. The energy difference between σ_g and σ_u is always smaller than the energy difference between σ_u and σ_g^*. This is a consequence of the inclusion of overlap in the calculation. Using perturbation theoretic reasoning (the energy denominator in Eq. 4) we expect that contribution from σ_g/σ_u mixing to total vibronic stabilization will be larger than the contribution from σ_u/σ_g^* mixing. The latter is not negligible, however, because the σ_u/σ_g^* gap is only 3 times larger than the σ_g/σ_u in case of the H_3 molecule (Fig. 9). And the AO coefficients in the σ_g^* are larger than in σ_g. Thus, we have to consider all three orbitals of H_3 in a qualitative picture of vibronic coupling.

Why and how do the atomic orbitals contributions in MOs of H_3 change as we move along Q_{as}? Let us trace the evolution of these orbitals step-by-step, using perturbational reasoning. In a first step we will move the AOs together with nuclei along Q_{as}. In a second step we interact the MOs so obtained (which are no longer solutions of the eigenvalue problem for the asymmetric system) to get new "true" MOs of asymmetric H_3. The two-step procedure described here is illustrated in Figs. 11a and 11b.

Consider first the mixing of σ_u into σ_g. As indicated schematically in Fig.11a, the geometrical perturbation increases bonding overlap between 1s (H_{center}) in σ_g and 1s (H_{right}) of σ_u (see arrows, 1s (H_{center}) in σ_g is closer to 1s (H_{right}) of σ_u). Therefore, (see bottom of Fig. 11b), σ_g mixes into itself σ_u with a positive sign (in a bonding way). The result (in σ_g) is to have the coefficient of H_{right} increase and that of H_{left} diminish.

Along Q_{as}, σ_u interacts with both σ_g and σ_g^*. σ_u mixes into itself σ_g with a negative sign (in an antibonding way, since it is the higher energy member of an interacting pair), and σ_g^* with a positive sign (in a bonding way, since σ_u is below σ_g^*) [43]. The net result is to have the H_{left} coefficient in σ_u grow, and that of H_{right} diminish.

Let us imagine now substitution of H_{center} by a more electronegative element (see Fig. 10). In this case, the contribution of 1s AO of H_{center} to σ_g is larger than for the unsubstituted H_3 molecule. Note that contributions of H_{left} and H_{right} to σ_u (very important for vibronic coupling) do not change upon substitution of H_{center}. Since the H_{ii} term in the perturbation expression depends on the coefficient products, in course of

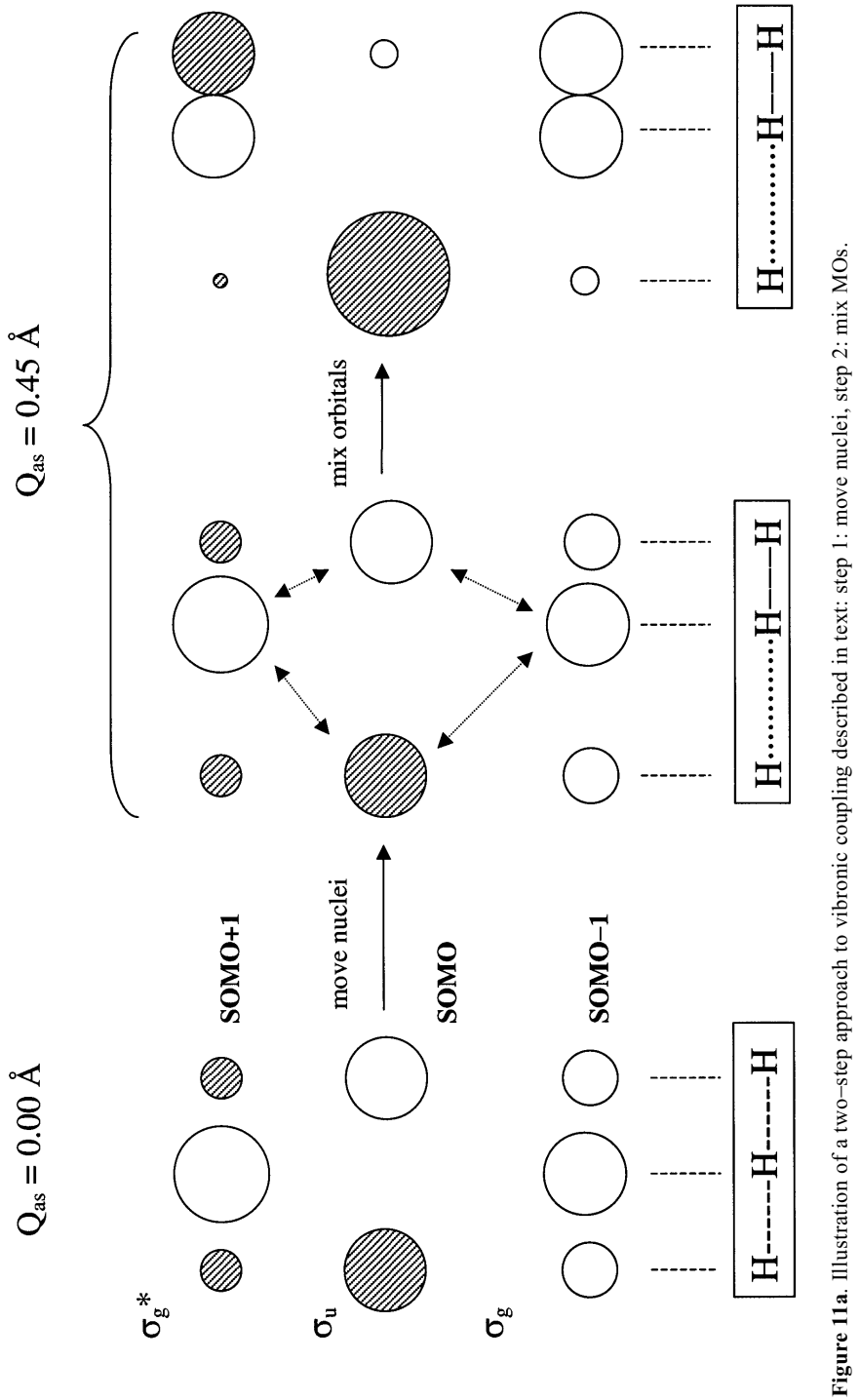

Figure 11a. Illustration of a two–step approach to vibronic coupling described in text: step 1: move nuclei, step 2: mix MOs.

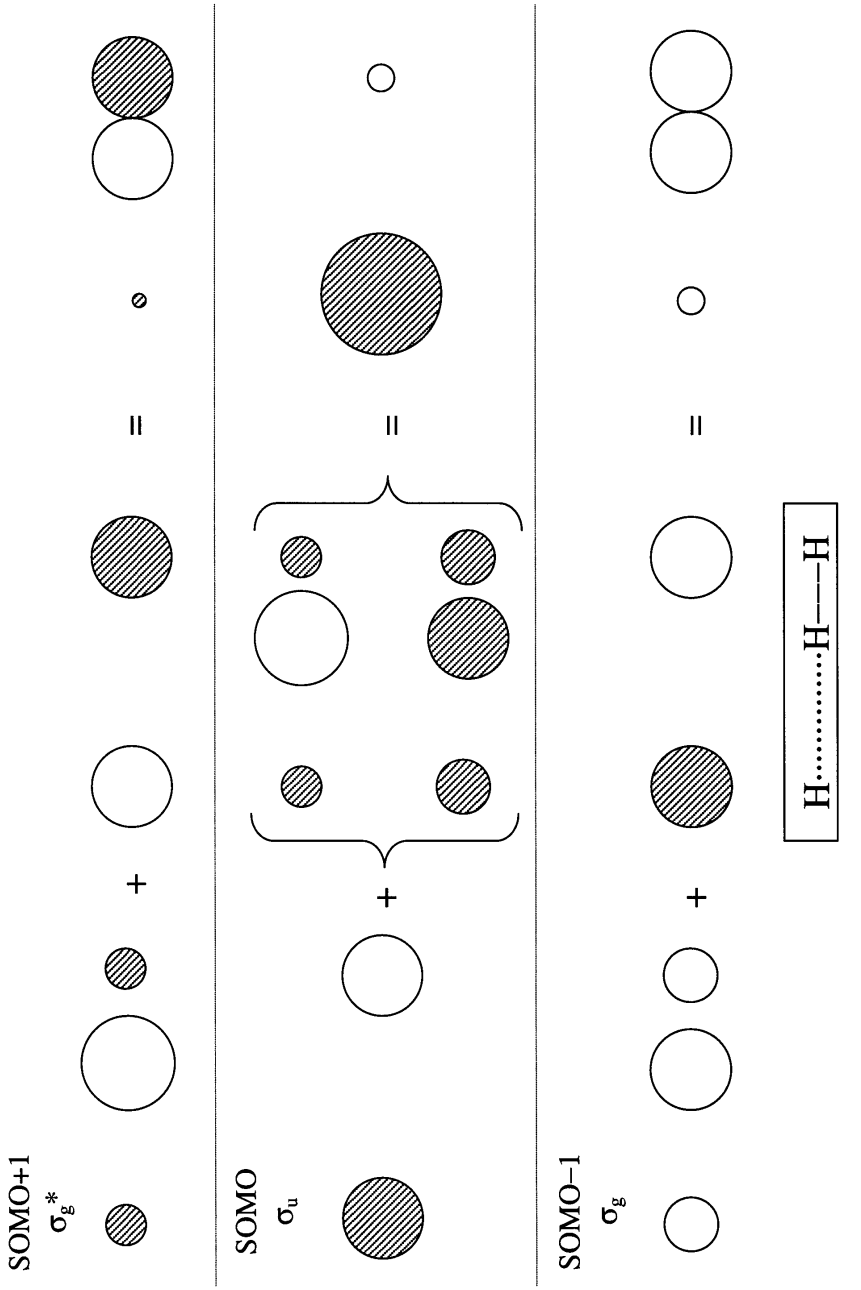

Figure 11b. Illustration of MOs mixing at Q_{as} = 0.45 Å (perturbational treatment of step 2).

molecular distortion along Q_{as} the overlap changes between 1s of H_{center} in σ_g and 1s of H_{right} and H_{left} in σ_u will be more pronounced in an H_2X than in an H_3 molecule. In this way, the vibronic coupling should be then stronger in H_2X molecules than in H_3. Applying the same line of thinking to H_2M molecules (H_{center} substituted by a more electropositive element) we can deduce that condition ii) will favor stronger vibronic coupling in "normal" H_3 over H_2M molecules.

As one can see from the above discussion, conditions i) and ii) have an *opposite* influence on vibronic stability, when H_{center} in H_3 is substituted by another element. What will be the net effect? It is difficult to answer this question without detailed computation. Hence, we have performed a series of EH calculations for an H_3 molecule varying the extended Hückel H_{ii} for the central H atom. In addition we have varied the H–H distance (preserving a symmetric linear arrangement of nuclei). In Fig. 12 we show a plot of k_u (force constant for the asymmetric stretching mode) *versus* the difference of H_{ii} between central and side H atom (ΔH_{ii}). Negative ΔH_{ii} in Fig. 12 implies that we are dealing with the "H_2M" case (center more electropositive), positive ΔH_{ii} with H_2X. The force constant has been computed here as square root of the stabilization energy. A formal negative sign has been introduced for the force constant if the corresponding computed frequency was imaginary.

We need to emphasize that k_u and not $\mathbf{G} = k_u/k_g$ is plotted in Fig. 12. The reason for that is that the EH cannot reliably compute k_g (the force constant for the symmetric stretching mode), and so rather than deal with errors in k_g influencing **G**, we have chosen to focus on k_u directly.

The influence of H_{center} substitution by another element, which differs in electronegativity which is predicted by EH (presented in Fig. 12), may be summarized as follows:

i) Substitution of H_{center} by a more electronegative element ($\Delta H_{ii} > 0$) strongly decreases the vibronic stability of the molecule.

ii) On the other hand, substitution of H_{center} by a more electropositive element ($\Delta H_{ii} < 0$) increases the vibronic stability of the molecule.

iii) Vibronic stability always decreases with bond length decrease, but the effect is not great. Although this feature agrees with the observation that molecules with large **f** (and thus with short bonds) are usually vibronically unstable, it might be also an artifact of the EHT [45].

Let us confront these predictions of EH (Fig. 12) with the results of actual quantum mechanical computations for triatomics. For this purpose we plot in Fig. 13 k_u (computed by DFT for a series of molecules) *versus* the difference of extended Hückel H_{ii} of the valence orbitals of elements constituting a given molecule. The difference in EH H_{ii} should be related to an electronegativity difference; we are reaching here for a relationship between the k_u or **G** *vs*. Δ EN plots shown earlier and an EH analogue.

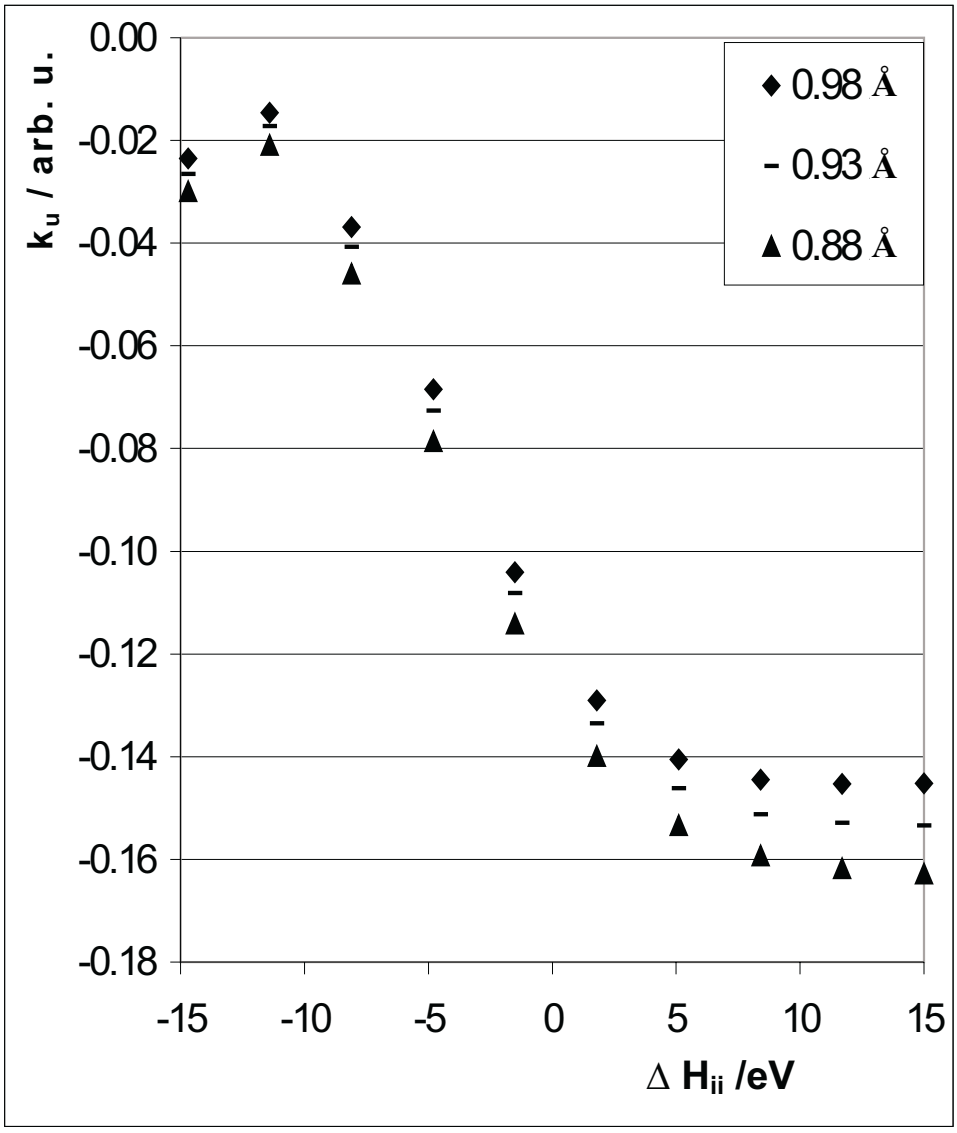

Figure 12. Plot of k_u (force constant for the asymmetric stretching mode) plotted versus the difference of Hückel parameters between central and side H atom (ΔH_{ii} /eV) in H′HH′ molecule; $\Delta H_{ii} = H_{ii}$ (H) – H_{ii} (H′). A standard value of H_{ii} (H′) = – 13.6 eV has been used. H_{ii} (H) has been varied in the – 13.6 eV ± 15.0 eV limits. Three cases are shown: $R_0 = 0.98$ Å, R0 = 0.93 Å, $R_0 = 0.88$ Å

There are some differences between EH predictions (Fig. 12) and results of the DFT computations (Fig. 13). This is not unexpected, since extended Hückel calculations are particularly poor for distances. Indeed, EH does not predict correctly the absolute values of k_u (k_u is always negative in EH, contrary to DFT computations). Might one at least trust the *trends* predicted by EH for k_u *vs*. Δ EN dependence and rationalize them?

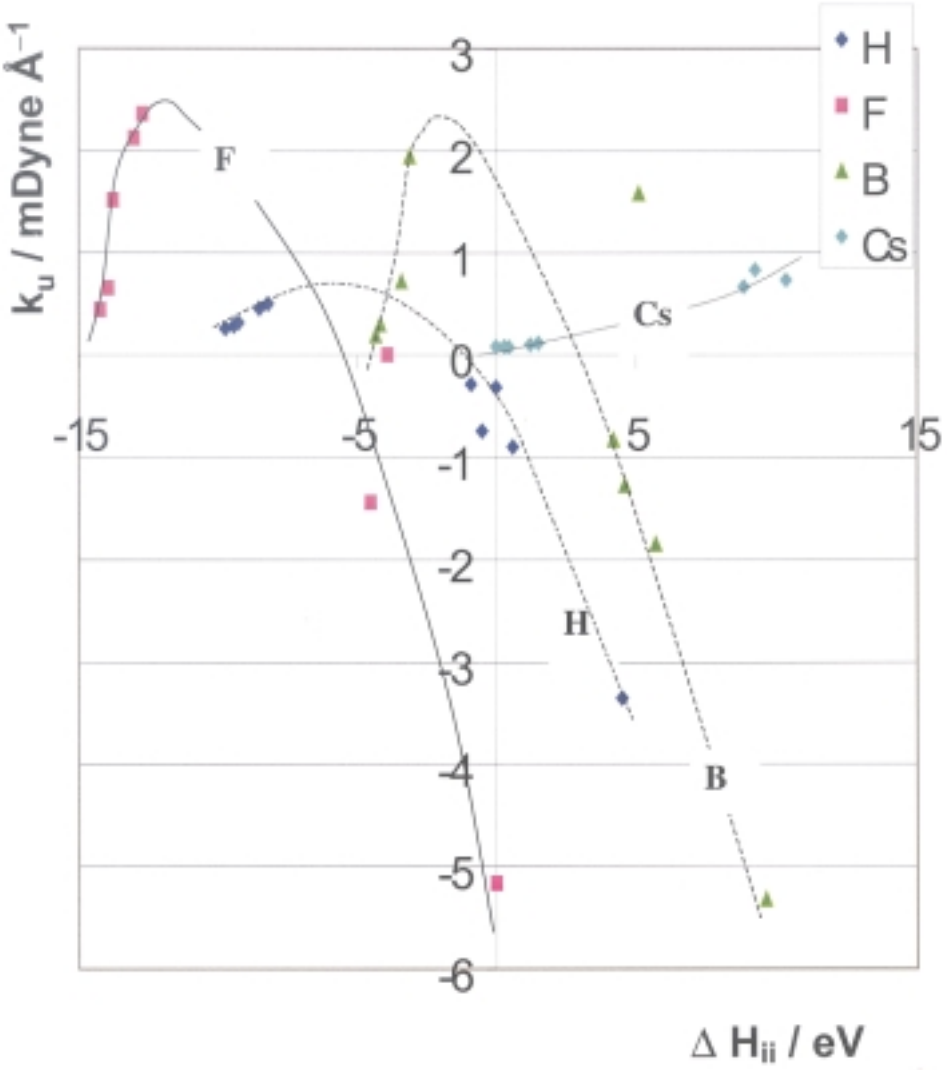

Figure 13. Plot of k_u for a series of A_2B linear symmetric molecules plotted versus the difference of extended Hückel H_{ii} parameters for valence orbitals of the central and side atom (ΔH_{ii}). The series are labeled by the element A in the A_2B molecule. For a more detailed description see text. Arbitrarily drawn lines have been introduced to guide an eye to trends for A = F, H, B, Cs.

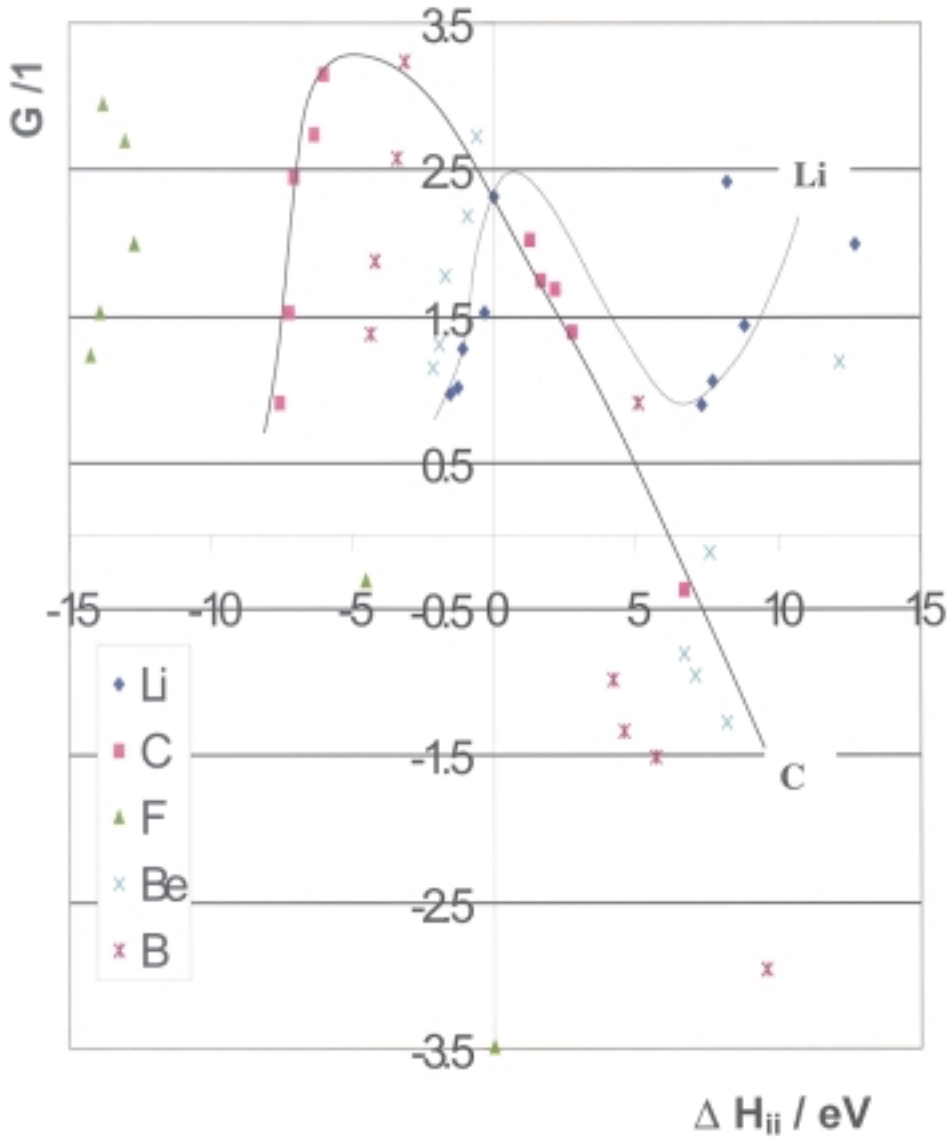

Figure 14. Plot of **G** for a series of A_2B linear symmetric molecules plotted versus the difference of extended Hückel H_{ii} parameters for valence orbitals of the central and side atom (ΔH_{ii}). The series is labeled by the element A in the A_2B molecule. For a more detailed description see text. Arbitrarily drawn lines have been introduced to guide an eye to trends for A = C, Li.

We think most of the trends are there in the EH model. A typical k_u *vs*. ΔH_{ii} dependence has usually a maximum at certain ΔH_{ii} (k_u here has been computed by DFT). This is similar to the **G** *vs*. ΔEN dependence, which we have discussed in a previous section (see Fig. 1). It is also similar to the **G** *vs*. ΔH_{ii} dependence (Fig. 14). Finally, this might also correspond to a small maximum observed at $\Delta H_{ii} \approx -12$ eV in the k_u *vs*. ΔH_{ii} dependence as calculated by EH (Fig. 12).

The most vibronically unstable species usually occur for the most positive values of ΔH_{ii} available for a given element A in an A_2B molecule (DFT result, Fig. 13). This is again very similar to the EH prediction (Fig. 12). The only exception from this rule is found for molecules containing typical metals such as alkalis. It is exemplified in Fig. 13 by the k_u *vs*. ΔH_{ii} dependence for Cs-containing species. The largest vibronic coupling (although not yet instability) is observed for Cs-containing intermetallics. How can we explain this discrepancy between DFT results and EH results in a simple qualitative way? We have to note that intermetallics have usually very small σ_g/σ_u and σ_u/σ^*_g gaps, in contrast to Cs-containing "salts". It seems that EH does not properly account for this class.

EH predicts a larger instability of ABA molecules relative to BAB molecules, where B is the more electronegative element. This is in good agreement with DFT results. EH also indicates a greater instability of molecules with shorter bonds. Indeed, DFT results show that molecules with large **f** (hence, often with short bonds, see Eq. 2) are the most vibronically unstable.

Summarizing this section, we think that on balance the extended Hückel ΔH_{ii} is of value in understanding qualitatively vibronic effects.

2.2. Vibronic Coupling and Molecular Hardness.

So far we have been studying quantitatively ABA molecules at a B3LYP/6-311++G** level of density functional theory. However, our qualitative explanatory approach was based on the EH method. It is interesting next to look qualitatively at vibronic coupling in triatomics within the DFT formalism. We will investigate particularly the relationship between the molecular hardness η and the vibronic stability parameter **G**.

In the very useful conception of Parr and Pearson, the hardness η [46,47] is defined in a consistent quantum mechanical way within density functional theory framework. Can we relate the results of our DFT calculations for particular molecules with η?

We have chosen H_2E and E_3 molecules as a subject of this study (E = F, Cl, Br, I, Li, Na, K, Rb, Cs). These 18 molecules range from highly unstable species, such as F_3 or H_2F, to very stable ones, such as Cs_3 or Li_2F. The approximate molecular hardness of E_3 and H_2E molecules has been calculated here as the weighted average of atomic hardnesses. Atomic hardness values were taken from [47].

Figure 15 plots the vibronic stability parameter **G** as a function of molecular hardness η for H_2E and E_3 families of triatomics.

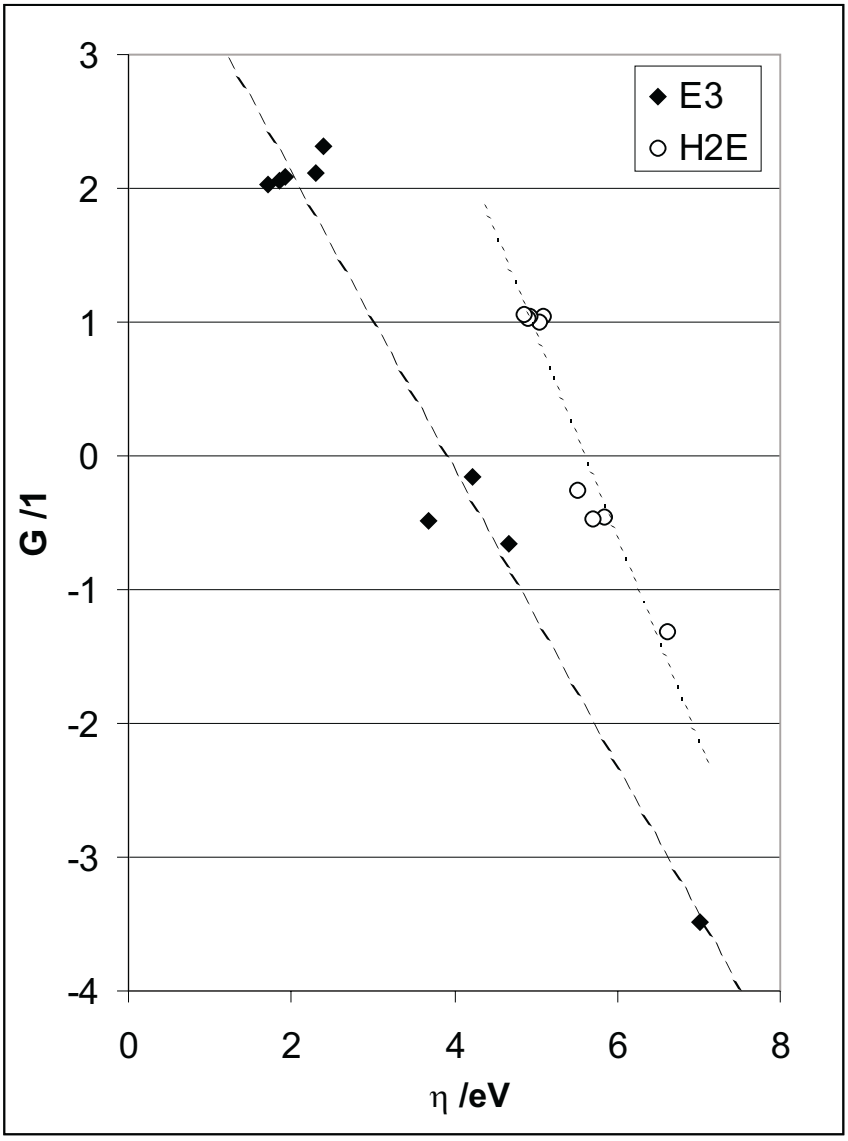

Figure 15. Plot of vibronic stability parameter **G** /1 versus the molecular hardness η /eV for two families of linear symmetric molecules: E_3 and H_2E (E = F, Cl, Br, I, Li, Na, K, Rb, Cs). The molecular hardness of E_3 and H_2E species has approximated here by a weighted average of atomic hardnesses. Dotted lines show linear regressions for E_3 and H_2E families.

A relationship between **G** and η seems to exist within each of the two families of molecules examined. Usually, the larger the η, the more negative the **G**, and the more unstable the molecule. The most negative values of **G** are always computed for the molecule with the largest η within a given family [48].

Thus our simple theoretical studies point to a strategy for increasing vibronic instability:

i) Molecular systems built of the hard Lewis acids and Lewis bases will usually exhibit large vibronic instability.
ii) Small molecules with low-lying contracted orbitals will usually exhibit substantial vibronic instability.

Of course, these are necessary, but not sufficient conditions for strong vibronic coupling (for example LiF_2 is vibronically stable, although it is built of pretty hard Lewis acids and bases). As we have learned elsewhere, substantial covalency (at best such orbitals matching, which provides a covalent-to-ionic curve crossing – see section 2.5) is also necessary for strong vibronic instability to occur.

We notice that conclusions i) and ii) agree well with computational (DFT) data presented in section 1.1. Interesting complementary results, buttressing our conclusions on the influence of softness and hardness, have been also obtained from studying the influence of a basis set choice on the vibronic stability (see Appendix B). This leaves us hope that vibronic effects, of a complex quantum-mechanical nature, may be relatively easily translated into chemical concepts. The parameter **f** used by us in this paper may be linked to chemical hardness, and such attempts are in progress [49].

Let us now turn to the relation of vibronic stability of A_2B molecules to the phenomenon of electron–rich bonding or hypervalence.

2.3. Vibronic Coupling and Hypervalence.

From a formal point of view, linear symmetric $ABA^{\bullet}$ molecules show three-center three-electron bonding. This feature locates them half way between the electron-poor A_2B^+ molecules and electron-rich A_2B^- ones (of the I_3^- type). The latter are characterized by four-electron three-center bonding and are typical hypervalent species [50]. In sections 2.1–2.2 we have tried to understand the factors governing the vibronic stability of $ABA^{\bullet}$ species. Now we would like to explore the hypervalence motif a little deeper.

A typical problem that we face dealing with a "fully" hypervalent system (*e.g.* I_3^-) is: will the system preserve symmetry (I--I--I$^-$), or will it become unsymmetrical (I$^-$·····I–I) [51]? This problem is very similar to one we studied for $ABA^{\bullet}$ species (*e.g.* such as I_3^0). And our previous experiences with vibronic stability – although initially inspired by the relevance of vibronic effects to superconductivity, might help us understand the factors influencing tendencies of "fully" hypervalent or electron–rich species towards asymmetrization.

We will use again the linear symmetric H_3 system as a simple model, concentrating on three species: H_3^-, H_3^0 and H_3^+. These serve us as models for electron-rich, neutral and electron-deficient molecules. Fig. 16 shows the energy levels in H_3^-, H_3^0 and H_3^+ molecules as calculated at the B3LYP/6-311++G** level of theory [52].

As may be seen from Fig. 16, the vibronic stability of H_3^-, H_3^0 and H_3^+ molecules differs substantially. Instability increases in the order: $H_3^+ \rightarrow H_3^0 \rightarrow H_3^-$; H_3^+ is stable along Q_{as} [53]. What are the most important reasons for these differences?

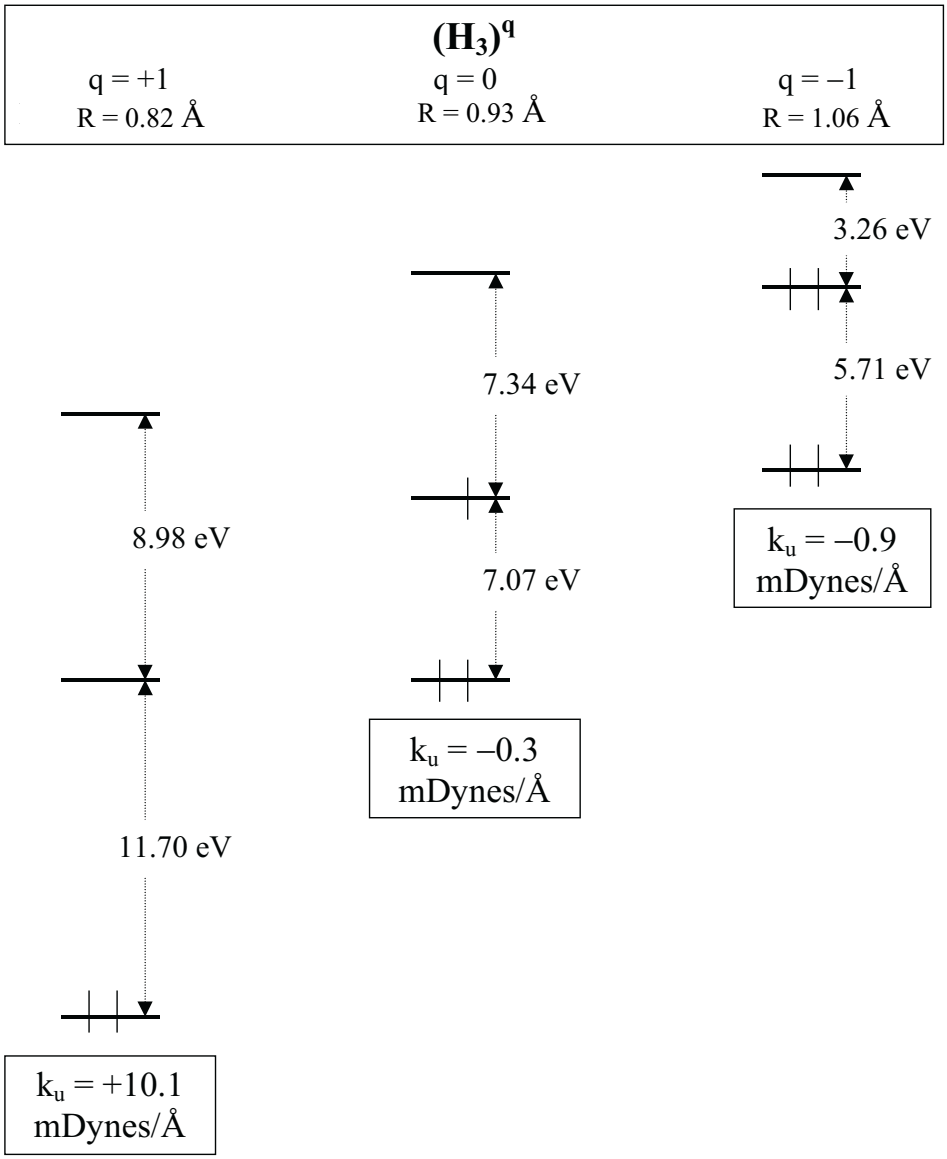

Figure 16. Energy levels in the linear symmetric H_3^-, H_3^0 and H_3^+ molecules as calculated at the B3LYP/6-311++G** level of theory. Optimized bond lengths R /Å and force constants for the asymmetric stretch k_u are given. The vertical scale is schematic.

Let us recall here Fig. 9, the simple EH model. The stabilization energy in H_3^0 asymmetrization comes mainly from the energy decrease of σ_g, and somewhat less so, σ_u. Hence, we can easily deduce that vibronic instability should indeed increase in order: $H_3^+ \rightarrow H_3^0 \rightarrow H_3^-$ due to occupation of σ_u by, respectively, zero, one and two electrons. An additional reason for the largest susceptibility of H_3^- towards asymmetrization is clear from the MO scheme given in Fig. 16. One can see that both σ_g/σ_u

and σ_u/σ_g^* gaps decrease strongly with increase of negative charge on H_3 skeleton. This means – as a perturbation theoretic approach tells us – that vibronic second order effects will be strongest in the H_3^- case.

The instability order $H_3^+ < H_3^0 < H_3^-$ we have obtained and understood for H_3 species might be transformed into a more general proposition: electron rich molecules will be more unstable towards asymmetrization than the corresponding electron-deficient molecules. Unfortunately, this simple rule is not generally valid. Consider for example the $F_3^+ \rightarrow F_3^0 \rightarrow F_3^-$ series. F_3^0 is unsymmetrical, while there is strong theoretical and experimental evidence that a linear F_3^- molecule is symmetric [54]. How could one explain this?

We tend to think about relative stability of linear symmetric F_3^- molecule in terms of s-p mixing. Although s-p mixing will be the subject of the next section, let us shortly explain its role here (see Figs. 17 and 18 for details). For F_3^- s-p mixing shows up through a nonzero contribution of a 2s orbital to SOMO. This makes SOMO antibonding with respect to neighboring F atoms. Subsequently, symmetric elongation of the F–F bonds will be driven by a greater force in F_3^- as compared to F_3^0. Having in mind the general rule that **G** is more negative for shorter bonds, we might qualitatively understand the stability trend in the F_3 series. The more diffuse character of F_3^- orbitals (as compared to F_3^0) and the larger polarizability also contribute to the symmetrization of the F_3^- molecule.

2.4. Hybridization, s-p Mixing and Vibronic Coupling.

To understand the interplay of hybridization and s-p mixing in vibronic effects we will use again a simple model based on EH considerations. We analyze the vibronic stability of a linear symmetric F_3 molecule, varying the extended Hückel H_{ii} of the 2s orbital of the central F atom (the H_{ii} of the 2p orbital remains constant). This way we will "steer" the s-orbital contribution to the three center bond orbitals and pass continuously from a 3 AO scheme (three 2p orbitals [55]) to a 4 AO one (one 2s and three 2p orbitals). Fig. 17 shows the calculated plot of k_u *versus* the difference of H_{ii} between the 2s and 2p orbital of the central F atom (ΔH_{ii} (sp)). Negative ΔH_{ii} (sp) means that 2s orbital is below the 2p one.

The shape of the k_u *versus* ΔH_{ii} (sp) dependence is very interesting. Apparently, there is a huge vibronic stability decrease in the region of strong s-p mixing. Interestingly, the largest instability is observed for ΔH_{ii} (sp) ≈ 2 and not for ΔH_{ii} (sp) $= 0$. Of course, the region of positive ΔH_{ii} (sp) corresponds to a very unphysical situation (s orbital above p) and we do not pay much attention to it. We are doing these numerical experiments not to model a real molecule, but as a kind of laboratory to turn on s,p mixing, spanning the range from little mixing to much.

In the reasonable range of negative ΔH_{ii} (sp), the important results is that the smaller the s-p gap, the larger the vibronic instability.

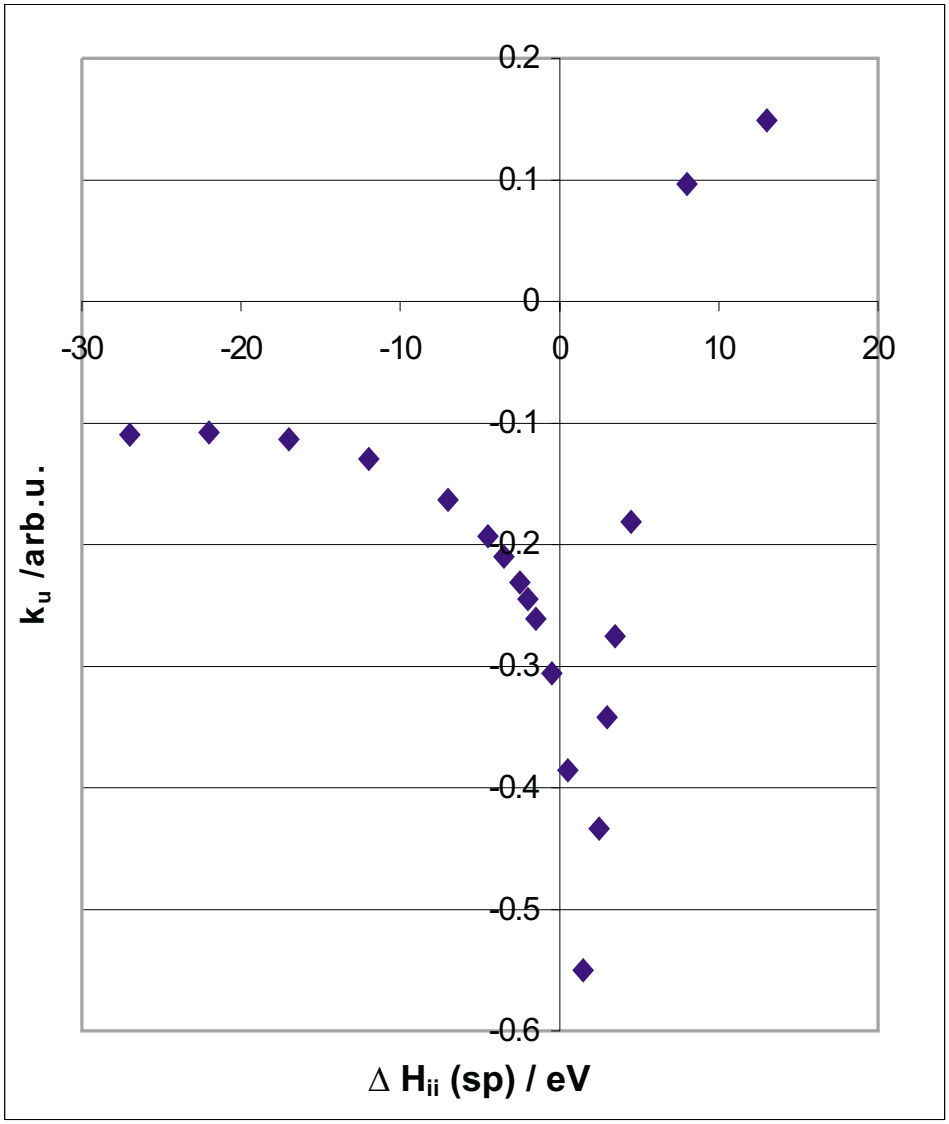

Figure 17. Plot of the force constant for the antisymmetric stretch (k_u) *versus* the difference of extended Hückel H_{ii} parameter between the 2s and 2p orbital of the central F atom (ΔH_{ii} (sp)), in the linear symmetric F_3 molecule. The theoretical results derive from an EH calculation.

We will now use a MO picture to explain the trend observed in Fig. 17.

The three-center system built of p orbitals at each atom (and interacting s orbitals) is a little different than the previously studied three s orbital system, so some introduction is needed. Fig. 18 shows the relevant orbitals before s-p mixing [56].

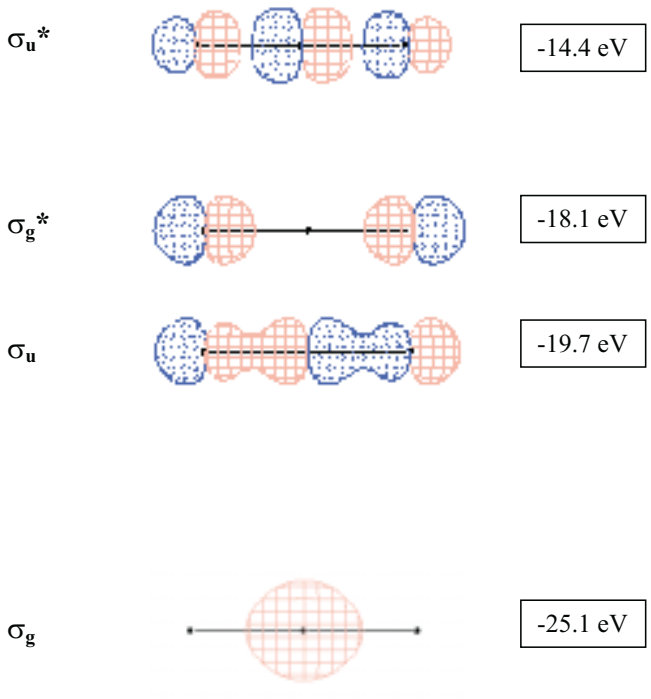

Figure 18. The MOs scheme of the linear symmetric F_3 system *before* turning on the s-p mixing for F_{center}. The case shown is for a 2s–2p gap of –7 eV. Two different shades of gray represent opposite phases of wavefunction.

Note that the SOMO is now σ_g in symmetry (and not σ_u as in the three s orbital case we studied earlier). The s orbital at the central atom has the same σ_g symmetry. The MO diagram is instructive for it tells us that the two σ_g orbitals (the low lying s and the SOMO) must interact, as long as there is any overlap between them. The net result will be a "repulsion" of the orbitals, the lower one will be F_{center}/F_{right} and F_{center}/F_{left} bonding, the upper antibonding. This is why we label them even here as σ_g and σ^*_g.

Fig. 19 shows the evolution of the σ-block of MOs in the vicinity of the SOMO for the linear symmetric F_3 molecule, as the extended Hückel H_{ii} for the 2s orbital of the central F atom is varied.

Analyzing Fig.19, we find the reasons for a strong dependence of the vibronic stability on the s-p mixing. Our analysis takes into account only the four σ orbitals in the vicinity of SOMO contributing substantially to the vibronic coupling along Q_{as}: σ_g, σ_u, σ^*_g, σ^*_u (see Fig. 18). The π-block of MOs does not mix with the s orbital of F_{center} due to symmetry [57]. Moreover, the contribution from the π orbitals (mixing themselves within π block) to the total vibronic coupling along Q_{as} is much smaller than that from σ.

It is clear from Fig. 19 that sp-hybridization plays important role in the vibronic coupling: admixture of the s orbital of F_{center} into σ^*_g increases significantly the energy changes associated with asymmetrization. The reasons for this in the case of F_3 are the following:

i) the 2s orbital of F_{center} mixes into SOMO (σ^*_g) in an antibonding way;
ii) following such mixing, the energy gap between σ^*_g and σ^*_u decreases, and the contribution of the s orbital of F_{center} to σ^*_g increases. This, in turn, enables more efficient σ^*_g/σ^*_u mixing after symmetry breaking (recall that such mixing is turned on for $Q_{as} \neq 0$);
iii) asymmetrization effectively creates sp hybrids at F_{center}.

Hence, the sp-mixing increases strongly the vibronic coupling in the $\Delta H_{ii}(sp) < 0$ region. The more distant (in energy) the lower-lying (occupied) 2s orbitals from the σ 2p orbitals, the larger the vibronic stability. This finding is in general agreement with what is known of the influence of s-p mixing on vibronic stability in many extended structures [58].

Let us now investigate the relationship of the s-p mixing to "ionic/covalent" curve crossing, and analyze the importance of the latter for vibronic coupling.

2.5. Avoided "Ionic/Covalent" Curve Crossing and the Vibronic Coupling.

The results presented in the previous section may also be interpreted using a language of ionic/covalent curve crossing.

It is clear from Fig. 19 that a "repulsion" of the σ_g orbitals occurs in the pseudo–F_3 molecule as the extended Hückel H_{ii} of the 2s orbital of the central F atom is varied (H_{ii} of the 2p orbital remains constant). This is emphasized by dotted curves in Fig. 19a. Both σ_g orbitals significantly change their character as a result. The lower energy σ_g orbital is dominated by a 2s contribution of the central F atom for $\Delta H_{ii}(sp) = -7$ eV, and by a 2p contribution of the side F atoms for $\Delta H_{ii}(sp) = +7$ eV. The reverse is true for the higher energy σ^*_g orbital. Clearly, a kind of curve crossing has taken place in this system.

We emphasize again that the region with 2s close to and especially above 2p is unphysical. Nevertheless, variation of the 2s-2p energy difference over a large range

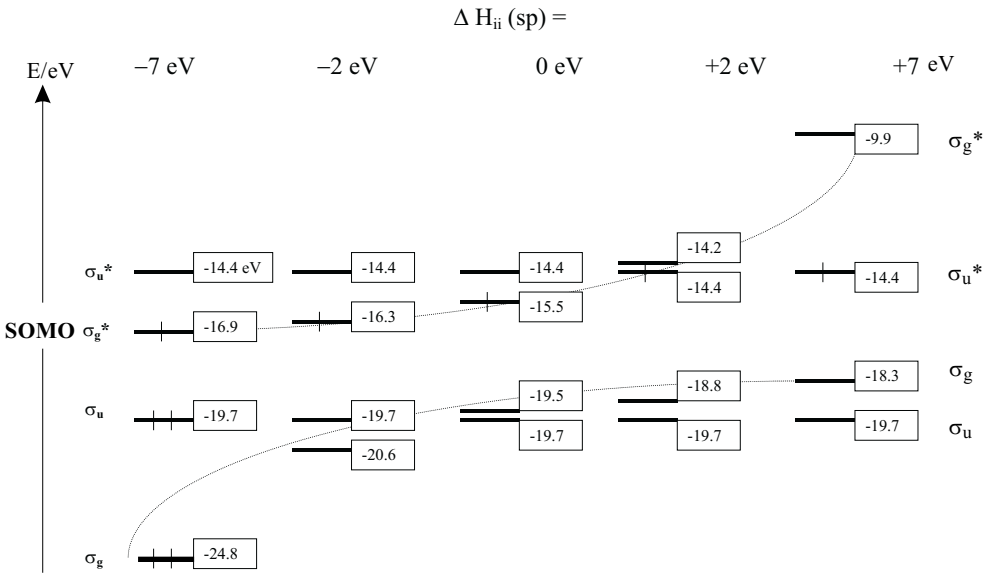

Figure 19a. Evolution of the MOs scheme of the linear symmetric F_3 system upon varying the extended Hückel H_{ii} parameter for the 2s orbital of the central F atom. The cases shown are for a 2s–2p gap (ΔH_{ii} (sp)) of –7 eV, –2 eV, 0 eV, +2 eV and +7 eV. For more details see text. "Repulsion" of the σ_g levels is illustrated schematically with dotted lines. Energy in eV.

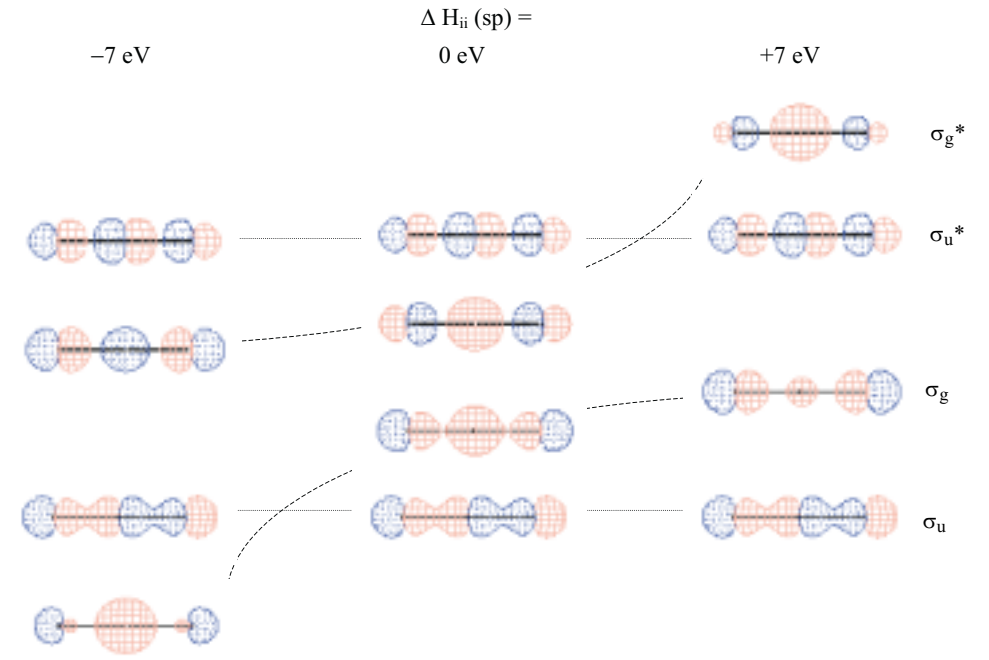

Figure 19b. Evolution of the MOs of the linear symmetric F_3 system upon varying the extended Hückel H_{ii} parameter for the 2s orbital of the central F atom. The cases shown are for a 2s–2p gap (ΔH_{ii} (sp)) of –7 eV, 0 eV and +7 eV.

is a useful way to tune s,p mixing. And this is what different elements in the periodic table do – vary the ns-np energy difference, even if ns is never above np.

Let us elaborate our argument for saying a curve crossing has taken place. Variation of the extended Hückel H_{ii} of the 2s orbital of the central F atom influences the electronegativity of the central F atom. The computed Mulliken charge on the central F atom is +0.30 e for ΔH_{ii} (sp) = –7 eV, and as much as +1.51e for ΔH_{ii} (sp) = +7 eV. It is a typical feature of the 4-electron hypervalent AAA systems that the central atom is positively charged relative to the end atoms [59]. A chemist is likely to assign electron occupation in the F–F–F system as:

$$s^2p^5, s^2p^5, s^2p^5 \quad \text{or} \quad F^0–F^0–F^0 \quad \text{for} \quad \Delta H_{ii}\,(sp) = -7\ eV \tag{5}$$

and

$$s^2p^6, s^0p^3, s^2p^6 \text{ or } F^{-1}–F^{+2}–F^{-1} \quad \text{for} \quad \Delta H^{ii}\,(sp) = +7\ eV \tag{6}$$

In other words, the "forbidden curve crossing" has the character of a "covalent–to–ionic transition"! And it enormously influences the vibronic stability of a molecule, as we have seen.

At this point two interesting and important theoretical contributions to the literature come to mind. In these the authors link the superconductivity phenomenon in the solid state either to "sudden polarization as a result of small geometrical distortion" (hypothetical organic superconductors, Salem 1966) [60], or directly to "ionic/covalent curve crossing" (oxocuprate materials, Burdett 1993) [2s].

In particular, Burdett discussed in some detail the possible influence of the "ionic/covalent curve crossing" on the "magic electronic state" in oxocuprate superconductors. He postulated that there are huge variations of the wavefunction with Cu–O distance in the "ionic/covalent curve crossing" region:

$$Cu^{3+} + O^{2-} \rightarrow Cu^{2+\bullet} + O^{-\bullet} \tag{7}$$

We feel that Burdett's hypothesis is of a particular importance for theoretical studies of the electronic structure of superconducting materials. The existence of a curve crossing region might lead to large variations in the nature of the computed wavefunction for the system, which might be forced towards either "ionic" or "covalent" configurations.

We have computed the vibronic stability of a symmetric linear $[Cu^{3+}–O^{2-}–Cu^{2+}]^{\bullet}$ species along an antisymmetric stretching coordinate, using EH. We have varied H_{ii} for the p orbital of the central O atom in a broad energy range so to model avoided crossing with Cu(d) orbitals; the procedure (and purpose) is analogous then to that applied for a pseudo-F_3 model. Varying O(p) orbital energy allows us tune Cu(d)/O(p) orbital mixing. Such mixing is known to occur in oxocuprate materials, and certainly

depends on the oxidation state of Cu. Strong increase in vibronic instability has been computed in the vicinity of the crossing region, as compared to the region where Cu(d)/O(p) mixing is small. While the increase was not as steep a function of H_{ii} as for the pseudo-F_3 molecule, yet the essence of the phenomenon was preserved.

Burdett's and Salem ideas can be transferred to the BCS theory of superconductivity [61]. States below and above the Fermi level, which are coupled in pairs through an optical phonon, are now in the "forbidden curve crossing region", and their coupling increases significantly. In this paper we have argued that "ionic/covalent curve crossing" dramatically influences the vibronic stability of a molecule [62]. An analogue of Burdett's idea thus is found for triatomic molecules, even at the extended Hückel level [63].

2.6. Vibronic Coupling and Resonance Structures.

Consider another approach to vibronic coupling. Let us think in terms of resonance structures, an archetypical concept in chemical language. Lines in resonance structures symbolize spin–coupled electron pairs localized in bonds or in lone pairs. Resonance structures are a classic tool that chemists use to describe qualitatively the electron distribution of molecules. Valence bond theory, in which the "resonance structures" terminology originates, also is the basis of a curve–crossing model [64]. Resonance structures and valence bond configurational thinking has been very successfully applied by Shaik and coworkers to studies of dynamics of the chemical reactions and properties of transition states. The quantitative approach presented in [64] allows a beautiful connection to be made between a singlet-triplet gap in A_2 diatomics and the gap between "repulsive" potential energy curves of symmetric A_3 triatomics. Inclusion of a low lying ligand-to-metal charge-transfer state increases the stability of a symmetric ("ionic") transition state and lowers the energy barrier for an A + BA $\rightarrow$ AB + A reaction.

We think that the studies of Shaik and coworkers are very much relevant to the description of systems exhibiting large vibronic coupling. It also becomes clear now why large vibronic coupling in T_1 states of interhalogen AB molecules [4] is likely to imply strong vibronic instabilities in interhalogen ABA open-shell systems [5].

CONCLUSIONS

We have concentrated our attention on the off-diagonal vibronic coupling. We have examined off-diagonal vibronic coupling in symmetric linear triatomic A_2B open-shell molecules, for the antisymmetric stretching mode. The triatomic A_2B molecules are usually classified into two groups: mixed-valence (MV) and intermediate-valence (IV) (using criteria of static/dynamic nonequal/equal charge distribution on two centers A), and they are ideal for studying vibronic coupling.

The vibronic stability of ABA molecules (as measured by the force constant of the antisymmetric stretching mode, k_u, as well as the "antisymmetric mode softening

parameter" **G**) has been studied. **G** is defined as the ratio of antisymmetric to symmetric stretching force constant; it is a very sensitive indicator of vibronic coupling. In this paper the range of A, B is very wide – element B originated from s, p, and A from s, p and d-blocks of the periodic table.

We have constructed maps of **G** in a space of two parameters: the difference of the Pauling electronegativity of A and B elements constituting A_2B molecule and the sum of the Pauling electronegativity for A and B. Alternatively, we have used the parameter **f** (**f** is defined as sum of electronegativities divided by AB bond length) instead of the sum of electronegativities. Our maps show that there exists a region of strong vibronic instability of A_2B molecules. This is observed for large values of **f** which are characteristic for small ABA molecules built of two nonmetallic p-block elements. ABA molecules containing a d-block element A are usually more vibronically stable than analogous molecules containing a p-block A element of same electronegativity.

Another interesting result of relevance to the vibrational spectra of A_2B molecules (see Appendix A) has been obtained: it appears that **f** correlates with the force constant for the symmetric stretching mode in certain families of linear symmetric triatomics.

Trying to rationalize the trends observed for h^i_{eg} in the space of certain "chemical" parameters, we constructed simple MO models, based on EH and DFT computations. We discuss h^i_{eg} in A_2B molecules in relevance to hypervalence, s-p mixing, "ionic/covalent curve crossing", and the hardness/softness of Lewis acids/bases. The most important general conclusions are the following:

i) Molecular systems built of hard Lewis acids/bases should be vibronically more unstable than systems built of soft Lewis acids/bases [65].

ii) The more pronounced s-p mixing, the larger the vibronic instability.

iii) An "ionic/covalent curve crossing" significantly increases the vibronic instability of a molecule.

Vibronic instability may be significant (*i.e.* may lead to geometrical instability of symmetrical molecular systems, with consequences for various observables) even for molecules with large energy gaps of about 10–15 eV (as in the case of the ammonia inversion [18]). The vibronic effects are most significant when states mixed (which are not necessarily nearest in energy) involve *strongly bonding or antibonding orbitals* (bonds are strongly weakened and/or strengthened during the molecular vibration). It is also known that vibronic effects are extremely important in both "classical" BCS [1] and high-temperature superconductivity [2]. In this paper we tried to show what might be the conditions for large vibronic instability [66].

Our theoretical findings may be important in the experimental search for new superconducting materials in solid state. It is still a long way from simple physical models and quantum mechanical computations for small molecules to the complex behavior of solids due to their collective electronic / magnetic phenomena. We will try to come part of this way in our next paper [5].

Acknowledgments

This research was conducted using the resources of the Cornell Theory Center, which receives funding from Cornell University, New York State, the National Center for Research Resources at the National Institutes of Health, the National Science Foundation, the Defense Department Modernization Program, the United States Department of Agriculture, and corporate partners. We were supported by the Cornell Center for Materials Research (CCMR), a Materials Research Science and Engineering Center of the National Science Foundation (DMR-9632275) and by NSF Research Grant (CHE 99-70089). Authors acknowledge Norman Goldberg and Mihaela Bojin for helpful comments.

Appendix A

*Utility of **f** for Predicting k_g.*

The qualitative correlation of parameter **f** with the force constant for the symmetric stretching mode (k_g) was discovered by us previously, for three families of ABA$^{\bullet}$ triatomics: intermetallics, interhalogens and salts [5,67]. We may elaborate a quantitative approach, based on the extensive calculations of this paper. Fig. 20 presents the plot of $\sqrt{k_g}$ *versus* parameter **f** for about 100 previously studied $AB_2^{\bullet}$ molecules [5].

There is a good monotonic correlation between $\sqrt{k_g}$ and **f**. The least square linear relationship found is: $\sqrt{k_g} = 0.344\ \mathbf{f} + 0.166$, with correlation coefficient $R^2 = 0.909$. Thus **f** correlates sufficiently well with

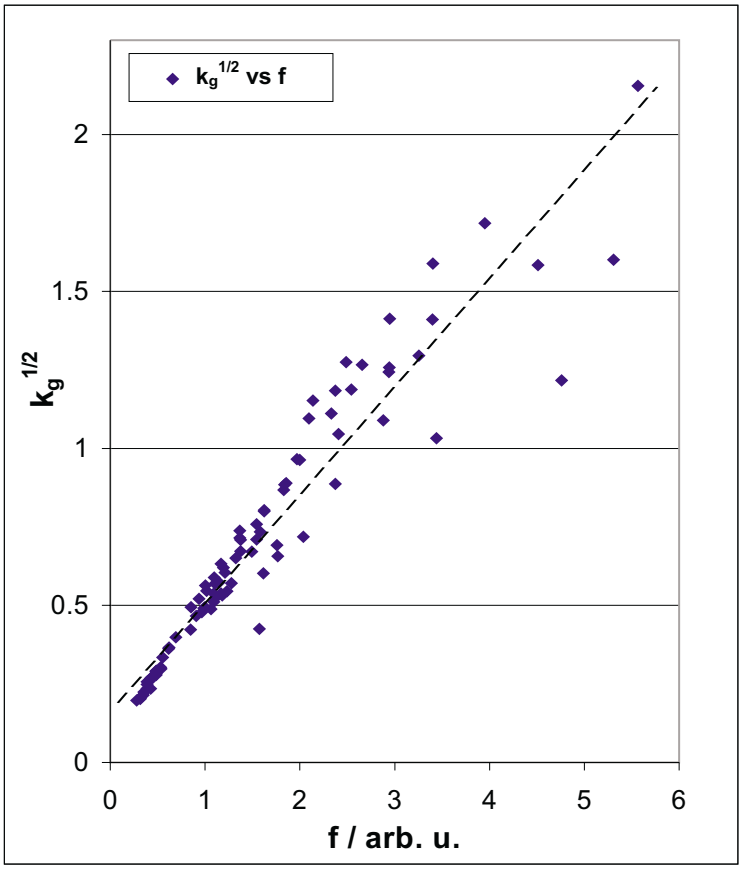

Figure 20. Linear least – squares correlation between $\sqrt{k_g}$ and parameter **f** for a broad family of about 100 linear symmetric triatomic radicals ($AB_2^{\bullet}$). The least-squares fitted linear curve is shown with dotted line.

the square root of the second derivative of the potential energy (*i.e.* force constant) [28]. We obtained also a good $\sqrt{k_g}$ *vs* **f** correlation for all 460 molecules studied in this paper (including those containing transition metal atoms). Note that **f** also correlates well with the first derivative of the potential energy (*i.e.* force) in certain families of diatomics [4]. It is impressive to us that a simple empirical parameter correlates so well with the results of complex quantum mechanical computations [68]. We think that **f** will prove useful for analyzing other molecular features as well.

Appendix B

Basis Set Effects in Vibronic Coupling – a DFT Picture.

There is another, indirect way to look at the role of softness and hardness in affecting vibronic stability. Let's look at the influence of the basis set on the vibronic stability parameter **G**. We have chosen H_2Cl as a subject of this study.

Adding polarization and diffuse function to the basis set on one hand is just an applied mathematical procedure to get a more accurate solution of the wave equation. But, we think that there is something physical and chemical to be learned from the effects of polarization and diffusion functions. Such basis set functions are especially important for systems with diffuse or low lying unoccupied orbitals. Electrons in such systems are usually easily polarizable and weakly bound. We think that one way to judge that a system is "hard" is if little addition of polarization and diffuse function to the basis set is necessary to describe it properly.

In Table 1 we list optimized bond length R_0, force constants for symmetric (k_g) and antisymmetric (k_u) stretching modes and vibronic stability parameter **G** for H_2Cl as computed at B3LYP level with different basis sets.

Table 1. Influence of the basis set choice on the optimized bond length R_0, force constants for symmetric (k_g) and antisymmetric (k_u) stretching modes and vibronic stability parameter **G** for H_2Cl as computed at DFT/B3LYP level.

basis set	R_0/Å	k_u/mdyne Å^{-1}	k_g/mdyne Å^{-1}	**G**/1
6-311++G**	1.50	–0.90	1.99	–0.45
6-31++G**	1.50	–0.91	1.99	–0.46
6-31+G**	1.50	–0.92	1.99	–0.47
6-31G**	1.50	–0.91	2.00	–0.45
6-31G*	1.51	–1.01	1.87	–0.54
6-31G	1.56	–0.96	1.64	–0.59
6-21G*	1.51	–1.05	1.82	–0.58
6-21G	1.57	–0.98	1.56	–0.63
4-31G*	1.52	–1.15	1.76	–0.65
4-31G	1.57	–0.98	1.58	–0.62
3-21G*	1.51	–1.08	1.76	–0.62
3-21G	1.57	–1.00	1.52	–0.66

It may be immediately seen from Table 1 that basis set choice has a small effect on the optimized bond length, but a substantial one on the parameter **G** for the symmetric linear H_2Cl molecule. We obtained the largest vibronic instability (**G** = –0.66) with the smallest basis set (3-21G), and the smallest vibronic instability (**G** = –0.45) with the largest basis set (6-311++G**). **G** increases upon inclusion of polarization functions (6-31G → 6-31G* → 6-31G**). The same is true for other families of basis sets. Apparently, progressive addition of polarization functions results in a *decrease* of the vibronic instability.

How **G** varies upon addition of diffuse functions is not very clear, nor as significant in the case of H_2Cl as for polarization functions. For basis sets: 6-31G**, 6-31+G**, and 6-31++G** we obtain **G** equal to –0.45, –0.47, and –0.46, respectively. The vibronic stability (**G**) changes only slightly upon progressive addition of diffuse functions.

The influence of the basis on computed **G** is substantial; the ratio of the smallest and the largest computed **G** value is large (~150%). Of course, linear H_2Cl is strongly vibronically unstable, so even a basis set that is too small does not result in a qualitative error (for all basis sets $\mathbf{G} << 0$). However, one may easily imagine cases for $\mathbf{G} \approx 0$, when an improper choice of basis might be the source of serious qualitative (stability or instability?) error.

We suggest that vibronic coupling is likely to be large in systems built of atoms for which addition of polarization and diffuse function to the basis set only slightly influences the computed vibronic stability parameters (*i.e*. of small, weakly polarizable atoms). Results of the above study may be thus nicely related to conclusions from section 2.2.

REFERENCES

1. Bardeen J., Cooper L.N. and Schrieffer J.R., *Phys. Rev.*, **108**, 175 (1957).
2. On the importance of vibronic effects (and generally: lattice–electron coupling) for superconductivity see: (I) oxocuprates: (a) Alexandrov A.S. and Edwards P.P., *Physica C*, **331**, 97 (2000), and references therein. (b) Burdett J.K. and Kulkarni G.V., *Phys. Rev. B*, **40**, 8908 (1989). (c) Jarlborg T., *Solid State Commun*., **67**, 297 (1988). (II) oxobismuthates: (d) Meregalli V. and Savrasov S.Y., *Phys. Rev. B*, **57**, 14453 (1998). (e) Navarro O. and Chavira E., *Physica C*, **282–287**, 1825 (1997). (f) Shirai M., Suzuki N. and Motizuki K., *J. Phys.: Condens. Matter.*, **2**, 3553 (1990). (III) fullerides: (g) Schluter M., Lanoo M., Needels M., Baraff G.A. and Tomanek D., *Phys. Rev. Lett*., **68**, 526 (1992). (h) Jishi R.A. and Dresselhaus M.S., *Phys. Rev. B*, **45**, 2579 (1992). (i) Novikov D.L., Gubanov V.A. and Freeman A.J., *Physica C*, **191**, 399 (1992). (j) Kresin V.Z., *Phys. Rev. B*, **46**, 14883 (1992). (k) Asai Y. and Kawaguchi Y., *Phys. Rev. B*, **46**, 1265 (1992). (l) Rai R., *Z. Phys. B*, **99**, 327 (1996). (IV) silicide clathrates: (m) Yoshizawa K., Kato T. and Yamabe T., *J. Chem. Phys*., **108**, 7637 (1998). (n) Yoshizawa K., Kato T., Tachibana M. and Yamabe T, *J. Phys. Chem. A*, **102**, 10113 (1998). (V) borocarbides: (o) Gompf F., Reichardt W., Schober H., Renker B. and Buchgeister M., *Phys. Rev. B: Condens. Matter.*, **55**, 9058 1997). (VI) mercury fluoroarsenates: (p) Slot J.J.M., Boon M. and Weger M., *Solid State Commun*., **56**, 645 (1985). On accuracy of BCS predictions for different classes of superconductors see: (r) B. Chakraverty, Ramakrishnan T., *Physica C*, **282–287**, 290 (1997). On the "magic electronic state" in oxocuprates and its connection to Cu-O bond stretching see: (s) Burdett J.K., *Inorg. Chem*., **32**, 3915 (1993).
3. Part 1, Grochala W., Konecny R. and Hoffmann R., *Chem. Phys*., **265**, 153 (2001).
4. Part 2, Grochala W. and Hoffmann R., *New J. Chem*., **25**, 108 (2001).
5. Part 3, Grochala W. and Hoffmann R., *J. Phys. Chem. A,* **104**, 9740 (2000).
6. In some sense our paper is analogous to the review on periodicity in 120 first- and second-row diatomic molecules, by Boldyrev A.I., Gonzales N. and Simons J., *J. Phys. Chem*., **98**, 9931 (1994).
7. Part 5, Grochala W., Hoffmann R. and Edwards P.P., manuscript in preparation.
8. Gaussian 94, Revision D.3, Frisch M.J., Trucks G.W., Schlegel H.B., Gill P.M.W., Johnson B.G., Robb M.A., Cheeseman J.R., Keith T., Petersson G.A., Montgomery J.A., Raghavachari K., Al-Laham M.A., Zakrzewski V.G., Ortiz J.V., Foresman J.B., Cioslowski J., Stefanov B.B., Nanayakkara A., Challacombe M., Peng C.Y., Ayala P.Y., Chen W., Wong M.W., Andres J.L., Replogle E.S. , Gomperts R., Martin R.L., Fox D.J., Binkley J.S., Defrees D.J., Baker J., Stewart J.P., Head-Gordon M., Gonzalez C. and Pople J.A., Gaussian, Inc., Pittsburgh PA, 1995.
9. HyperChem 5.0, Hypercube, Inc. Ltd.
10. Landrum G.A.,"YAEHMOP: Yet Another extended Hückel Molecular Orbital Package." A package for performing EH calculations on molecules and extended systems and visualizing the results. (1995) YAeHMOP is freely available for both Unix workstations and Power Macintosh systems on the WWW at URL http://overlap.chem.cornell.edu:8080/yaehmop.html.

11. C.A.C.A.O. (Computer Aided Composition of Atomic Orbitals), A Package of Programs for Molecular Orbital Analysis [PC Beta-Version 5.0 , 1998], Mealli C. and Proserpio D.M., with a major contribution by Ienco A., *J. Chem. Educ*., **67**, 399 (1990).
12. The reader is referred to several classical texts on vibronic coupling in triatomic and multiatomic molecules, whose importance was brought to our attention by a reviewer: (a) Öpik U. and Pryce M.H.L., *Proc. Roy. Soc. A*, **238**, 425 (1957); (b) Bader R.F.W., *Mol. Phys*., **3**, 137 (1960); (c) Bader R.F.W., *Canad. J. Chem*., **40**, 1164 (1962); (d) Köppel H., Domcke W., and Cederbaum L.S., *Adv. Chem. Phys*., **57**, 59 (1984); (e) Bersuker I.B. and Polinger V.Z., *Vibronic Interactions in Molecules and Crystals*, Springer-Verlag: Berlin, 1989; (f) Wong K.Y. and Schatz P.N., A Dynamic Model for Mixed-Valence Compounds. *Progress in Inorganic Chemistry, vol. 28*; Lippard S.J. Ed.; John Wiley and Sons: NY 1981; p.369; (g) Bersuker I.B., T*he Jahn-Teller Effect and Vibronic Interactions in Modern Chemistry*, Plenum Press: NY 1984. Theoretical models accompanied by calculations of vibronic stability for some "real" organic and inorganic molecules are presented in these papers.
13. As shown in Table S2 in Supplement, we could not compute 8 of 100 molecules in this family. The reasons for failure varied: problems with convergence, failures of Coulomb series, and density matrix breaking symmetry problems.
14. As shown in Table S2 in Supplement, we also could not compute 29 of the additional 240 molecules in this family. The reasons, as mentioned in Ref. 13, varied.
15. (a) Murphy L.R., Meek T.L., Allred A.L. and Allen L.C., *J. Phys. Chem. A*, **104**, 5867 (2000). (b) Cao C.Z., Li Z.L. and Allen L.C., *Chin. J. Inorg. Chem*., **15**, 218 (2000). On configuration energies, a modern concept related to electronegativity, see for example: (c) Mann J.B., Meek T.L. and Allen L.C., *J. Am. Chem. Soc*., **122**, 2780 (2000). (d) Mann J.B., Meek T.L., Knight E.T., Capitani J.F. and Allen L.C., *J. Am. Chem. Soc*., **122**, 5132 (2000).
16. Pauling L., *J. Am. Chem. Soc*., **54**, 3570 (1932).
17. Luo Y.-R. and Benson S.W., *J. Phys. Chem*., **94**, 914 (1990).
18. Khadikar P.V. and Pandharkar S., *Japan. J. Appl. Phys*., **27**, 2183 (1988).
19. Thomas T.D., *J. Am. Chem. Soc*., **92**, 4184 (1970).
20. Prasad P.L. and Singh S., *J. Chem. Phys*., **66**, 162 (1977).
21. Han W.-P. and Ai M., *J. Catalysis*, **78**, 281 (1982).
22. (a) Van Arkel A.E., *Molecules and Crystals in Inorganic Chemistry*; Interscience: NY, 1956.
(b) Ketlaar J.A.A., *Chemical Constitution, An Introduction to the Theory of the Chemical Bond*, 2nd ed., Elsevier: NY, 1958.
23. (a) Timoten R.S., Seetula J.A., Niiranen J. and Gutman D., *J. Phys. Chem*., **95**, 4009 (1991). (b) Schaefer T. and Hutton H.M., *Canad. J. Chem*., **45**, 3153 (1967). (c) Davies A.G., Smith L. and Smith P.J., *J. Organomet. Chem*., **23**, 135 (1970).
24. (a) Parr R.G. and Pearson R.G., *J. Am. Chem. Soc*., **150**, 7512 (1983). For the maximum hardness principle, see, for example: (b) Pearson R.G., *J. Chem. Educ*., **76**, 267 (1999).
25. (a) Gázquez J.L, *J. Phys. Chem. A*, **101**, 9464 (1997). (b) Pearson R.G., *J. Am. Chem. Soc*., **110**, 7684 (1988).
26. Mooser E. and Pearson W., *Acta Crystallogr.*, **12**, 1015 (1959).
27. Shankar S. and Parr R.G., *Proc. Natl. Acad. Sci. USA*, **82**, 264 (1985).
28. The Pauling electronegativity (PEN) has been used in this paper to compute **f**. Since PEN has formally units of square root of energy, **f** has units of square root of energy per distance. This might explain why a correlation of **f** with square root of the force constant (see Fig. 12) is almost linear (square root of force constant also has square root of energy per distance units). There is another electronegativity definition, the Mulliken electronegativity (MEN, expressed in energy units). MEN correlates quite well with PEN for most of elements. **f** would formally have energy per distance, *i.e*. force units if one defined **f** using MEN. Note that we obtained a strongly nonlinear correlation between **f** and force in Ref. 4.
29. Pearson R.G., *J. Molec. Struct*., **300**, 519 (1993).
30. As far as we know, there is no experimental data available for the symmetric linear radicals investigated in this paper. Such radicals are often not bound, and dissociate to a diatomic and an isolated atom. The species studied here might also be intermediates or transition states between two asymmetric linear, or two symmetric bent minima (these minima would correspond to "real" ground state molecules). Our study is not intended to predict the geometry of molecular radicals, but to discern trends in vibronic coupling.

31. Dissociation of symmetric linear triatomic proceeds along a combination of antisymmetric and symmetric stretching coordinates. In this paper we study the potential energy surface of a triatomic along an antisymmetric stretching coordinate, with symmetric stretching coordinate optimized and then frozen.
32. This study does not include closed–shell linear symmetric triatomics, such as *e.g.* CO_2. The presence of an unpaired electron in the species studied here usually results in strong vibronic coupling in these systems, in contrast to the closed–shell ones.
33. An unequal distribution of points in the ABA and BAB regions contributes partially to the left-right asymmetry of Fig. 3, but is not its main cause.
34. It has to be mentioned that k_g for all triatomics investigated in this paper also correlates very well with **f**.
35. Haddon R.C., *Acc. Chem. Res*., **25**, 127 (1992).
36. (a) Mattheiss L.F. and Hamann D.R., *Phys. Rev. Lett*., **60**, 2681 (1988). (b) Cava R.J., Batlogg B., Krajewski J.J., Farrow R., Rupp L.W., White A.E., Short K., Peck W.F. and Kometani T., *Nature*, **332**, 814 (1988).
37. Bednorz J.G. and Müller K.A., *Z. Phys. B*, **64**, 189 (1986).
38. Yamanaka S., Hotehama K. and Kawaji H., *Nature*, **392**, 580 (1998).
39. As Table S2 details, we could not compute properly 24 among 120 molecules in this group.
40. The only exception is Ir_2Li, which surprisingly is computed to be vibronically unstable.
41. Bally T. and Borden W.T., Calculations on Open-Shell Molecules: A Beginner's Guide, *Rev. Comput. Chem*., vol. 13, Lipkowitz K.B., Boyd D.B., Eds.; John Wiley and Sons: NY, 1999, p.1.
42. The difference of extended Hückel H_{ii} between 5s of Cs and 2p of F is about 15 eV, except F bonding is mainly through 2p.
43. Hoffmann R., *Acc. Chem. Res*., **4**, 1 (1971).
44. A general perturbation theory for a one–electron LCAO-MO method, including change of the overlap integrals, has been developed by Imamura (Imamura A., *Mol. Phys*., **15**, 225 (1968)).
45. We will discuss this point further in Ref. 7.
46. Parr R.G. and Pearson R.G., *J. Am. Chem. Soc*., **105**, 1503 (1983).
47. Pearson R.G., *Inorg. Chem*., **27**, 734 (1988).
48. We note that our results agree well with recent data on vibronic stability of planar triangular closed-shell AX_3 molecules (A = N to Bi, X = H, F to I): (a) Atanasov M. and Reinen D., *J. Phys. Chem. A*, **105**, 5450 (2001); (b) 15th International Jahn-Teller Symposium "Vibronic Interactions in Crystals and Molecules", Boston, 2000, Atanasov M. and Reinen D., *Chem. Eur. J.*, submitted. The authors conclude that the hardest molecules are the most susceptible to vibronic coupling (hardness is used by them in the chemical sense of Pearson's hardness η).
49. Ayers P.W. and Parr R.G., personal communication, 2000.
50. Some people see red when "hypervalence" is mentioned. We find this term to be heuristically useful and use it interchangeably with three–center four–electron bonding.
51. (a) Feretti V., Gilli P., Bertolasi V. and Gilli G., *Crystallogr. Rev.*, **5**, 3 (1996); (b) Bürgi H.-B. and Dunitz J.D., Eds. *Structure Correlation*, vol. 1; VCH: Weinheim, 1994; (c) Akiba K., *Chemistry of Hypervalent Compounds*; Wiley – VCH: NY, 1999, Chapter 1; (d) Musher J.I., *Angew. Chem. Int. Ed. Engl*., **8**, 54 (1969).
52. A formal negative sign has been introduced for the force constant if the corresponding computed frequency is imaginary.
53. Of course, H_3^+ wants to be triangular. But in the spirit of our studies we keep it linear here.
54. (a) Cahill P.A., Dykstra C.E. and Martin J.C., *J. Am. Chem. Soc*., **107**, 6359 (1985). (b) Novoa J.J., Mota F. and Alvarez S., *J. Phys. Chem*., **92**, 6561 (1988). (c) Ault B.S., Andrews L., *Inorg. Chem*., **16**, 2024 (1977). (d) Landrum G.A., Goldberg N. and Hoffmann R., *J. Chem. Soc., Dalton Trans*., 3605 (1997).
55. We use here an approximate (three p orbitals) instead of a more correct picture (three p orbitals + two s orbitals at F_{left} and F_{right}), since the s–p mixing at F_{left} and F_{right} is relatively small, and not relevant to our discussion.
56. There is some s-p mixing at the terminal F's, which "shapes" these orbitals a little.
57. The s orbital of central F atom does contribute to the vibronic coupling along the normal coordinate for bending, however.
58. (a) Papoian G. and Hoffmann R., *Angew. Chem. Int. Ed*., **39**, 2408 (2000); (b) Ienco A, Hoffmann R. and Papoian G., *J. Am. Chem. Soc*., submitted.
59. This might be the reason why the "negative peak" in Fig. 13 does not occur for $\Delta H_{ii}(sp) = 0$, but for some positive value of $\Delta H_{ii}(sp)$.

60. Salem L., *Molec. Phys*., **11**, 499 (1966).
61. It is significant that avoided crossing seems to be important for such different superconducting materials as samarium sulphide, SmS (Varma C.M., *Rev. Mod. Phys*., **48**, 218 (1976)) and oxocuprates (Ref. 2s). Independent calculations confirm the hypothesis of dual character of the wavefunction for oxobismuthates, as well (Pyper N.C. and Edwards P.P., in: Polarons and Bipolarons in High-T_C Superconductors and Related Materials, ed. by Salje E.K.H, Alexandrov A.S. and Liang W.Y., Cambridge University Press, Cambridge 1995).
62. One should consider in a more rigorous approach also nonadiabatic corrections, which are important in the vicinity of curve–crossing region.
63. Of course, the model used by us to simulate "ionic/covalent curve crossing" may be substituted by other approaches. A rigorous model for an ABA triatomic should show how the "ionic/covalent curve crossing" along the symmetric stretching coordinate influences the vibronic stability along the antisymmetric stretching coordinate.
64. (a) Shaik S.S. and Shurki A., *Angew. Chem. Int. Ed*., **38**, 586 (1999). (b) Maitre P., Hiberty P.C., Ohanessian G. and Shaik S.S., *J. Phys. Chem*., **94**, 4089 (1990).
65. Large vibronic instability for systems with deep lying, contracted orbitals suggests the potential utility of a Hamilton population analysis (HP) for analysis of vibronic coupling (see for example HP *vs* H_{ii} dependence in: Glassey W.V. and Hoffmann R., *J. Chem. Phys*., **113**, 1698 (2000).
66. From both computations and theoretical models we know how to reach the goal of large vibronic coupling. However, there is a limit to the extent and significance of large vibronic coupling. This limit is determined by the thermodynamic stability of a molecule toward asymmetric dissociation. If the coupling is so large that it leads to an ABA molecule's dissociation (such dissociation proceeds along a combination of antisymmetric and symmetric stretching coordinates), then that coupling in a way has no real physical importance. A linear symmetric structure (the point at which **G** is determined) is then too far away from any real equilibrium geometry. Hence, "prodissociative", enormously large coupling constants might not be useful in pointing to molecules which may have interesting properties.
67. The increase of the experimental force constants in the order $I_2 < Br_2 < Cl_2 < F_2$, $Rb_2 < K_2 < Na_2 < Li_2$, and HI < HBr < HCl < HF, has been noted, and an interesting correlation of the force constants with dissociation energies has been introduced (Nakamoto K., Infrared and Raman Spectra of Inorganic and Coordination Compounds, 3rd Ed., John Wiley and Sons: NY, Chichester, Brisbane, Toronto, 1978).
68. We have made some progress toward a physical justification of the use of **f**; this work will be published elsewhere.

Supplement – Tables

Table S1. Calculated geometric, vibrational and vibronic parameters for linear $ABA^{\bullet}$ molecules where A, B = s, p – block element: optimized A–B bond length (R_0/Å), force constant for the symmetric (k_g/mDyne $Å^{-1}$) and antisymmetric stretching (k_u/mDyne $Å^{-1}$), and vibronic stability parameter (**G**/1). Sum and difference of electronegativities between A and B ($EN_A + EN_B$, and Δ EN, respectively), parameter **f** [arb.u.], difference of Hückel parameters for A and B valence orbitals ($\Delta E_{Hückel}$/eV), and $\sqrt{k_g}$ (arb.u.) are also shown. Molecules are grouped following main groups of the periodic table. Negative values of k_u and **G** indicate imaginary frequency for antisymmetric stretch.

molecule	Δ EN	$EN_A + EN_B$	R_0/Å	k_g/mDyne $Å^{-1}$	k_u/mDyne $Å^{-1}$	**G**/1	**f**/ arb.u.	$\Delta E_{Hückel}$/ eV	$\sqrt{k_g}$/ arb.u
Group 1									
H_2F	1.9	6.1	1.149	2.562	–3.354	–1.31	5.31	4.5	1.60
H_2Cl	0.9	5.1	1.500	1.991	–0.901	–0.45	3.40	0.6	1.41
H_2Br	0.7	4.9	1.664	1.582	–0.747	–0.47	2.94	–0.5	1.26
H_2I	0.4	4.6	1.809	1.410	–0.291	–0.26	2.54	–0.9	1.19

Table S1 (continuation)

H_3	0.0	4.2	0.931	2.510	–0.322	–0.13	4.51	0.0	1.58
H_2Li	–1.1	3.1	1.763	0.479	0.501	1.05	1.76	–8.2	0.69
H_2Na	–1.2	3.0	2.012	0.450	0.452	1.00	1.49	–8.5	0.67
H_2K	–1.2	3.0	2.434	0.298	0.313	1.05	1.23	–9.26	0.55
H_2Rb	–1.3	2.9	2.608	0.275	0.282	1.03	1.11	–9.42	0.52
H_2Cs	–1.4	2.8	2.799	0.245	0.259	1.06	1.00	–9.72	0.49
Li_2F	3.0	5.0	1.682	1.366	2.714	1.99	2.97	12.7	1.17
Li_2Cl	2.0	4.0	2.158	0.792	1.134	1.43	1.85	8.8	0.89
Li_2Br	1.8	3.8	2.338	0.646	0.680	1.05	1.63	7.7	0.80
Li_2I	1.5	3.5	2.562	0.512	0.455	0.89	1.37	7.3	0.72
Li_2H	1.1	3.1	1.574	0.932	2.242	2.41	1.97	8.2	0.97
Li_3	0.0	2.0	2.885	0.159	0.367	2.31	0.69	0.0	0.40
Li_2Na	–0.1	1.9	3.090	0.131	0.199	1.52	0.61	–0.3	0.36
Li_2K	–0.1	1.9	3.571	0.092	0.118	1.28	0.53	–1.06	0.30
Li_2Rb	–0.2	1.8	3.740	0.084	0.085	1.01	0.48	–1.22	0.29
Li_2Cs	–0.3	1.7	3.995	0.072	0.069	0.96	0.43	–1.52	0.27
Na_2F	3.1	4.9	2.034	1.093	2.885	2.64	2.41	13.0	1.05
Na_2Cl	2.1	3.9	2.524	0.575	1.289	2.24	1.55	9.1	0.76
Na_2Br	1.9	3.7	2.690	0.502	0.822	1.64	1.38	8.0	0.71
Na_2I	1.6	3.4	2.908	0.400	0.496	1.24	1.17	7.6	0.63
Na_2H	1.2	3.0	2.01*	***			1.50	8.5	
Na_2Li	0.1	1.9	3.069	0.134	0.261	1.95	0.62	0.3	0.37
Na_3	0.0	1.8	3.256	0.112	0.236	2.11	0.55	0.0	0.33
Na_2K	0.0	1.8	3.723	0.081	0.168	2.07	0.48	–0.76	0.28
Na_2Rb	–0.1	1.7	3.884	0.074	0.111	1.50	0.44	–0.92	0.27
Na_2Cs	–0.2	1.6	4.138	0.066	0.087	1.32	0.39	–1.22	0.26
K_2F	3.1	4.9						13.86	
K_2Cl	2.1	3.9	2.949	0.424	1.159	2.73	1.32	9.86	0.65
K_2Br	1.9	3.7	3.096	0.385	0.921	2.39	1.20	8.76	0.62
K_2I	1.6	3.4	3.348	0.299	0.578	1.93	1.02	8.36	0.55
K_2H	1.2	3.0	2.46*				1.22	9.26	
K_2Li	0.1	1.9	3.552	0.089	0.161	1.81	0.53	1.06	0.30
K_2Na	0.0	1.8	3.721	0.078	0.153	1.96	0.48	0.76	0.28
K_3	0.0	1.8	4.223	0.055	0.115	2.09	0.43	0	0.23

Table S1 (continuation)

K_2Rb	–0.1	1.7	4.360	0.055	0.098	1.78	0.39	–0.16	0.23
K_2Cs	–0.2	1.6	4.613	0.046	0.069	1.50	0.35	–0.46	0.21
Rb_2F	3.2	4.8						13.92	
Rb_2Cl	2.2	3.8	3.140	0.365	0.892	2.44	1.21	10.02	0.60
Rb_2Br	2.0	3.6	3.281	0.347	0.929	2.68	1.10	8.92	0.59
Rb_2I	1.7	3.3	3.533	0.271	0.685	2.53	0.93	8.52	0.52
Rb_2H	1.3	2.9	2.652	0.290	0.468	1.61	1.09	9.42	0.54
Rb_2Li	0.2	1.8	3.718	0.085	0.142	1.67	0.48	1.22	0.29
Rb_2Na	0.1	1.7	3.876	0.071	0.121	1.70	0.44	0.92	0.27
Rb_2K	0.1	1.7	4.359	0.055	0.101	1.84	0.39	0	0.23
Rb_3	0.0	1.6	4.500	0.050	0.103	2.06	0.36	0.16	0.22
Rb_2Cs	–0.1	1.5	4.761	0.042	0.084	2.00	0.32	–0.3	0.20
Cs_2F	3.3	4.7	2.76*				1.70	14.22	
Cs_2Cl	2.3	3.7	3.349	0.324	0.728	2.25	1.10	10.32	0.57
Cs_2Br	2.1	3.5	3.485	0.317	0.827	2.61	1.00	9.22	0.56
Cs_2I	1.8	3.2	3.748	0.244	0.663	2.72	0.85	8.82	0.49
Cs_2H	1.4	2.8	2.89*					9.72	
Cs_2Li	0.3	1.7	3.985	0.071	0.112	1.58	0.43	1.52	0.27
Cs_2Na	0.2	1.6	4.145	0.062	0.098	1.58	0.39	1.22	0.25
Cs_2K	0.2	1.6	4.622	0.046	0.072	1.56	0.35	0.46	0.21
Cs_2Rb	0.1	1.5	4.764	0.041	0.078	1.90	0.31	0.3	0.20
Cs_3	0.0	1.4	5.026	0.039	0.079	2.03	0.28	0	0.20
Group 2									
Be_2F	2.5	5.5	1.529	2.320	2.743	1.18	3.60	12.1	1.52
Be_2Cl	1.5	4.5	2.101	0.955	–1.215	–1.27	2.14	8.2	0.98
Be_2Br	1.3	4.3	2.298	0.792	–0.749	–0.95	1.87	7.1	0.89
Be_2I	1.0	4.0	2.511	0.692	–0.557	–0.81	1.59	6.7	0.83
Be_2H	0.6	3.6	1.578	0.937	–0.112	–0.12	2.28	7.6	0.97
Be_2Li	–0.5	2.5	2.619	0.234	0.636	2.72	0.95	–0.6	0.48
Be_2Na	–0.6	2.4	2.936	0.168	0.367	2.18	0.82	–0.9	0.41
Be_2K	–0.6	2.4	3.485	0.098	0.173	1.77	0.69	–1.66	0.31
Be_2Rb	–0.7	2.3	3.707	0.076	0.099	1.30	0.62	–1.92	0.28
Be_2Cs	–0.8	2.2	3.974	0.064	0.073	1.14	0.55	–2.12	0.25

Table S1 (continuation)

Mg_2F	2.8	5.2						9.1	
Mg_2Cl	1.8	4.2	2.488	0.657	0.364	0.55	1.69	5.2	0.81
Mg_2Br	1.6	4.0	2.688	0.558	0.206	0.37	1.49	4.1	0.75
Mg_2I	1.3	3.7	2.920	0.446	0.056	0.13	1.27	3.7	0.67
Mg_2H	0.9	3.3						4.6	
Mg_2Li	–0.2	2.2	3.111	0.113	0.268	2.37	0.71	–3.6	0.34
Mg_2Na	–0.3	2.1	3.456	0.069	0.192	2.78	0.61	–3.9	0.26
Mg_2K	–0.3	2.1	4.108	0.033	0.090	2.73	0.51	–4.66	0.18
Mg_2Rb	–0.4	2.0	4.367	0.024	0.049	2.04	0.46	–4.92	0.15
Mg_2Cs	–0.5	1.9	4.729	0.014	0.025	1.79	0.40	–5.12	0.12
Ca_2F	3.0	0.05						11.99	
Ca_2Cl	2.0	4.0	2.826	0.571	1.17	2.05	1.42	8.09	0.76
Ca_2Br	1.8	3.8	3.012	0.466	0.941	2.02	1.26	6.99	0.68
Ca_2I	1.5	3.5	3.301	0.346	0.491	1.42	1.06	6.59	0.59
Ca_2H	1.1	3.1						7.49	
Ca_2Li	0.0	2.0	3.195	0.187	0.352	1.88	0.63	–0.71	0.43
Ca_2Na	–0.1	1.9	3.838	0.072	0.174	2.42	0.50	–1.01	0.27
Ca_2K	–0.1	1.9	4.475	0.037	0.107	2.89	0.42	–1.77	0.19
Ca_2Rb	–0.2	1.8	4.695	0.033	0.082	2.48	0.38	–2.03	0.18
Ca_2Cs	–0.3	1.7	5.001	0.026	0.054	2.08	0.34	–2.23	0.16
Sr_2F	3.0	5.0						11.48	
Sr_2Cl	2.0	4.0	2.983	0.52	1.044	2.01	1.34	7.58	0.72
Sr_2Br	1.8	3.8	3.154	0.433	1.114	2.57	1.20	6.48	0.66
Sr_2I	1.5	3.5	3.448	0.315	0.717	2.28	1.02	6.08	0.56
Sr_2H	1.1	3.1						6.98	
Sr_2Li	0.0	2.0	3.361	0.167	0.296	1.77	0.60	–1.22	0.41
Sr_2Na	–0.1	1.9	4.083	0.056	0.115	2.05	0.47	–1.52	0.24
Sr_2K	–0.1	1.9	4.783	0.027	0.071	2.63	0.40	–2.28	0.16
Sr_2Rb	–0.2	1.8	4.975	0.025	0.071	2.84	0.36	–2.54	0.16
Sr_2Cs	–0.3	1.7	5.317	0.019	0.054	2.84	0.32	–2.74	0.14
Ba_2F	3.1	4.9						n.d.**	
Ba_2Cl	2.1	3.9	3.157	0.45	0.892	1.98	1.24	n.d.	0.67
Ba_2Br	1.9	3.7	3.308	0.415	1.117	2.69	1.12	n.d.	0.64
Ba_2I	1.6	3.4	3.607	0.302	0.814	2.70	0.94	n.d.	0.55

Table S1 (continuation)

Ba_2H	1.2	3.0						n.d.	
Ba_2Li	0.1	1.9	4.083	0.061	0.101	1.66	9.47	n.d.	0.25
Ba_2Na	0.0	1.8	4.317	0.051	0.093	1.82	0.42	n.d.	0.23
Ba_2K	0.0	1.8	5.019	0.029	0.067	2.31	0.36	n.d.	0.17
Ba_2Rb	–0.	1.7	5.210	0.022	0.059	2.68	0.33	n.d.	0.15
Ba_2Cs	–0.2	1.6	5.580	0.017	0.048	2.82	0.29	n.d.	0.13
Group 13									
B_2F	2.0	6.0	1.546	1.799	–5.32	–2.96	3.88	9.6	1.34
B_2Cl	1.0	5.0	1.981	1.232	–1.852	–1.50	2.52	5.7	1.11
B_2Br	0.8	4.8	2.189	0.954	–1.274	–1.34	2.19	4.6	0.98
B_2I	0.5	4.5	2.367	0.854	–0.832	–0.97	1.90	4.2	0.92
B_2H	0.1	4.1	1.366	1.737	1.578	0.91	3.00	5.1	1.32
B_2Li	–1.0	3.0	2.025	0.599	1.937	3.23	1.48	–3.1	0.77
B_2Na	–1.1	2.9	2.690	0.28	0.721	2.58	1.08	–3.4	0.53
B_2K	–1.1	2.9	3.330	0.16	0.299	1.87	0.87	–4.16	0.40
B_2Rb	–1.2	2.8	3.556	0.135	0.186	1.38	0.79	–4.32	0.37
B_2Cs	–1.3	2.7						–4.62	
Al_2F	2.5	5.5	1.897	1.553	0.573	0.37	2.90	11.6	1.25
Al_2Cl	1.5	4.5	2.432	0.748	0.025	0.03	1.85	7.7	0.86
Al_2Br	1.3	4.3	2.654	0.628	0.102	0.16	1.62	6.6	0.79
Al_2I	1.0	4.0	2.848	0.516	0.105	0.20	1.40	6.2	0.72
Al_2H	0.6	3.6						7.1	
Al_2Li	–0.5	2.5	2.814	0.233	0.631	2.71	0.89	–1.1	0.48
Al_2Na	–0.6	2.4	3.106	0.190	0.616	3.24	0.77	–1.4	0.44
Al_2K	–0.6	2.4	3.845	0.114	0.289	2.54	0.62	–2.16	0.34
Al_2Rb	–0.7	2.3	4.065	0.103	0.190	1.85	0.57	–2.32	0.32
Al_2Cs	–0.8	2.2	4.012	0.079	0.128	1.62	0.55	–2.62	0.28
Ga_2F	2.4	5.6	1.991	1.231	0.475	0.39	2.81	11.35	1.11
Ga_2Cl	1.4	4.6	2.539	0.648	0.215	0.33	1.81	7.45	0.80
Ga_2Br	1.2	4.4	2.730	0.604	0.460	0.76	1.61	6.35	0.78
Ga_2I	0.9	4.1	2.947	0.488	0.334	0.68	1.39	5.95	0.70
Ga_2H	0.5	3.7						8.85	
Ga_2Li	–0.6	2.6	2.817	0.212	0.529	2.50	0.92	–1.35	0.46
Ga_2Na	–0.7	2.5	3.107	0.179	0.512	2.86	0.81	–1.65	0.42

Table S1 (continuation)

Ga_2K	–0.7	2.5	3.858	0.111	0.267	2.41	0.65	–2.41	0.33
Ga_2Rb	–0.8	2.4	4.058	0.098	0.205	2.09	0.59	–2.57	0.31
Ga_2Cs	–0.9	2.3						–2.87	
In_2F	2.3	5.7						11.9	
In_2Cl	1.3	4.7	2.687	0.599	0.395	0.66	1.75	8.01	0.77
In_2Br	1.1	4.5	2.949	0.488	–0.193	–0.40	1.53	6.91	0.70
In_2I	0.8	4.2	3.101	0.444	0.441	0.99	1.35	6.51	0.66
In_2H	0.4	3.8	1.977	0.782	1.025	1.31	1.92	7.41	0.88
In_2Li	–0.7	2.7	3.112	0.197	0.355	1.80	0.87	–0.79	0.44
In_2Na	–0.8	2.6	3.237	0.162	0.430	2.65	0.80	–1.09	0.40
In_2K	–0.9	2.5	3.993	0.105	0.227	2.16	0.63	–1.85	0.32
In_2Rb	–0.9	2.5	4.196	0.092	0.106	1.15	0.60	–2.11	0.30
In_2Cs	–1.0	2.4	4.223	0.090	0.282	3.13	0.57	–2.31	0.30
Tl_2F	2.2	5.8	2.393	0.887	0.549	0.62	2.42	12.3	0.94
Tl_2Cl	1.2	4.8	2.841	0.559	0.621	1.11	1.69	8.4	0.75
Tl_2Br	1.0	4.6	3.019	0.518	0.722	1.39	1.52	7.3	0.72
Tl_2I	0.7	4.3	3.235	0.405	0.594	1.47	1.33	6.9	0.64
Tl_2H	0.3	3.9	2.136	0.638	0.919	1.44	1.83	7.8	0.80
Tl_2Li	–0.8	2.8	2.989	0.178	0.365	2.05	0.94	–0.4	0.42
Tl_2Na	–0.9	2.7	3.263	0.159	0.399	2.51	0.83	–0.7	0.40
Tl_2K	–1.0	2.6	3.894	0.095	0.246	2.59	0.67	–1.46	0.31
Tl_2Rb	–1.0	2.6	4.083	0.085	0.244	2.87	0.64	–1.62	0.29
Tl_2Cs	–1.1	2.5	4.340	0.077	0.239	3.10	0.58	–1.92	0.28
Group 14									
C_2F	1.5	6.5	1.453	2.666	–0.980	–0.37	4.47	6.7	1.63
C_2Cl	0.5	5.5	1.671	3.147	4.393	1.40	3.29	2.8	1.77
C_2Br	0.3	5.3	1.913	2.020	3.519	1.74	2.77	1.7	1.42
C_2I	0.0	5.0	2.061	1.946	3.924	2.02	2.43	1.3	1.39
C_2H	–0.4	4.6	1.121	3.769	6.341	1.68	4.11	2.2	1.94
C_2Li	–1.5	3.5	1.961	0.787	2.476	3.15	1.79	–6	0.89
C_2Na	–1.6	3.4	2.430	0.416	1.140	2.74	1.40	–6.3	0.64
C_2K	–1.6	3.4	2.835	0.299	0.730	2.44	1.20	–7.06	0.55
C_2Rb	–1.7	3.3	3.188	0.230	0.349	1.52	1.04	–7.22	0.48
C_2Cs	–1.8	3.2	3.523	0.213	0.195	0.92	0.91	–7.52	0.46

Table S1 (continuation)

Si_2F	2.2	5.8	1.875	1.742	–0.025	–0.014	3.04	8.9	1.32
Si_2Cl	1.2	4.8	2.209	1.338	3.150	2.354	2.13	5	1.16
Si_2Br	1.0	4.6	2.420	1.069	1.694	1.585	1.86	3.9	1.03
Si_2I	0.7	4.3	2.719	0.728	0.121	1.166	1.55	3.5	0.85
Si_2H	0.3	3.9						4.4	
Si_2Li	–0.8	2.8	2.441	0.431	1.252	2.905	1.15	–3.8	0.66
Si_2Na	–0.9	2.7	2.917	0.264	0.758	2.871	0.93	–4.1	0.51
Si_2K	–0.9	2.7	3.579	0.202	0.484	2.391	0.75	–4.86	0.45
Si_2Rb	–1.0	2.6	3.806	0.175	0.298	1.703	0.68	–5.02	0.42
Si_2Cs	–1.1	2.5	4.091	0.147	0.201	1.367	0.61	–5.32	0.38
Ge_2F	2.2	5.8	1.973	1.752	2.069	1.181	2.94	9.1	1.32
Ge_2Cl	1.2	4.8	2.452	0.992	0.672	0.677	1.96	5.2	1.00
Ge_2Br	1.0	4.6	2.577	0.965	2.248	2.330	1.79	4.1	0.98
Ge_2I	0.7	4.3	2.869	0.652	0.454	0.696	1.50	3.7	0.81
Ge_2H	0.3	3.9	1.595	1.852	3.486	1.882	2.45	4.6	1.37
Ge_2Li	–0.8	2.8	2.531	0.365	0.973	2.666	1.11	–3.6	0.61
Ge_2Na	–0.9	2.7	2.931				0.92	–3.9	
Ge_2K	–0.9	2.7	3.642	0.196	0.452	2.306	0.74	–4.66	0.44
Ge_2Rb	–1.0	2.6	3.849	0.175	0.396	2.263	0.68	–4.82	0.42
Ge_2Cs	–1.1	2.5	4.130	0.147	0.314	2.136	0.61	–5.12	0.38
Sn_2F	2.25	5.75	2.117	1.401	1.492	1.065	2.72	9.78	1.18
Sn_2Cl	1.25	4.75	2.640	0.775	0.596	0.769	1.80	5.88	0.88
Sn_2Br	1.05	4.55	2.752	0.836	1.866	2.232	1.65	4.78	0.91
Sn_2I	0.70	4.25	2.936	0.705	1.719	2.438	1.45	4.38	0.84
Sn_2H	0.35	3.85	1.774	1.518	2.812	1.852	2.17	5.28	1.23
Sn_2Li	–0.75	2.75	2.684	0.323	0.873	2.703	1.02	–2.92	0.57
Sn_2Na	–0.85	2.65	3.095	0.230	0.582	2.530	0.86	–3.22	0.48
Sn_2K	–0.95	2.55	3.600	0.154	0.414	2.688	0.71	–3.98	0.39
Sn_2Rb	–0.95	2.55	3.947	0.117	0.246	2.103	0.65	–4.24	0.34
Sn_2Cs	–1.05	2.45	4.314	0.132	0.301	2.280	0.57	–4.44	0.36
Pb_2F	2.2	5.8	2.200	1.319	1.260	0.955	2.64	10.1	1.15
Pb_2Cl	1.2	4.8	2.30*					6.2	
Pb_2Br	1.0	4.6	2.873	0.688	0.789	1.147	1.60	5.1	0.83
Pb_2I	0.7	4.3	2.971	0.687	1.649	2.400	1.45	4.7	0.83

Table S1 (continuation)

Pb_2H	0.3	3.9	1.816	1.400	2.630	1.879	1.31	5.6	1.18
Pb_2Li	–0.8	2.8	2.961				0.95	–2.6	
Pb_2Na	–0.9	2.7	3.121				0.87	–2.9	
Pb_2K	–1.0	2.6	3.625	0.144	0.361	2.507	0.72	–3.66	0.38
Pb_2Rb	–1.0	2.6	4.004	0.108	0.206	1.907	0.65	–3.82	0.33
Pb_2Cs	–1.1	2.5	4.225	0.100	0.203	2.030	0.59	–4.12	0.32
Group 15									
N_2F	1.0	7.0	1.433	3.482	1.856	0.533	4.88	4.7	1.87
N_2Cl	0.0	6.0	1.533	4.905	10.061	2.051	3.91	0.8	2.21
N_2Br	–0.2	5.8	1.836	2.728	3.642	1.335	3.16	–0.3	1.65
N_2I	–0.5	5.5	1.943	2.768	2.540	0.918	2.83	–0.7	1.66
N_2H	–0.9	5.1	1.046	5.257	10.337	1.966	4.88	0.2	2.29
N_2Li	–2.0	4.0	1.881	0.948	2.814	2.968	2.13	–8	0.97
N_2Na	–2.1	3.9	2.238	0.505	1.198	2.372	1.74	–8.3	0.71
N_2K	–2.1	3.9	2.839	0.361	0.697	1.931	1.37	–9.06	0.60
N_2Rb	–2.2	3.8	3.054	0.301	0.404	1.342	1.24	–9.22	0.55
N_2Cs	–2.3	3.7	3.148	0.257	0.371	1.444	1.18	–9.52	0.51
P_2F	1.9	6.1	1.805	2.304	2.533	1.100	3.38	4.1	1.52
P_2Cl	0.9	5.1	2.174	1.595	–0.827	–0.518	2.35	0.2	1.26
P_2Br	0.7	4.9	2.337				2.10	–0.9	
P_2I	0.4	4.6	2.519				1.83	–1.3	
P_2H	0.0	4.2						–0.4	
P_2Li	–1.1	3.1	2.318	0.581	1.719	2.959	1.34	–8.6	0.76
P_2Na	–1.2	3.0	2.787	0.377	0.951	2.522	1.08	–8.9	0.61
P_2K	–1.2	3.0	3.367	0.247	0.585	2.368	0.89	–9.66	0.50
P_2Rb	–1.3	2.9	3.488				0.83	–9.82	
P_2Cs	–1.4	2.8	3.715	0.18	0.324	1.800	0.75	–10.12	0.42
As_2F	2.0	6.0	1.979	1.873	1.702	0.909	3.03	5.94	1.37
As_2Cl	1.0	5.0	2.311	1.348	2.909	2.158	2.16	2.04	1.16
As_2Br	0.8	4.8	2.529				1.90	0.94	
As_2I	0.5	4.5	2.940	0.694	–0.512	–0.738	1.53	0.54	0.83
As_2H	0.1	4.1	1.534	2.367	4.471	1.889	2.67	1.44	1.54
As_2Li	–1.0	3.0	2.559	0.482	1.005	2.085	1.17	–6.76	0.69
As_2Na	–1.1	2.9	2.890	0.344	0.74	2.151	1.00	–7.06	0.59

Table S1 (continuation)

As_2K	–1.1	2.9	3.454	0.238	0.555	2.332	0.84	–7.82	0.49
As_2Rb	–1.2	2.8	3.653	0.217	0.514	2.369	0.77	–7.98	0.47
As_2Cs	–1.3	2.7	3.755	0.195	0.519	2.662	0.72	–8.28	0.44
Sb_2F	2.1	5.9	2.127	1.656	1.82	1.099	2.77	6.4	1.29
Sb_2Cl	1.1	4.9						2.5	
Sb_2Br	0.9	4.7	2.719				1.73	1.4	
Sb_2I	0.6	4.4	3.124	0.605	–0.329	–0.544	1.41	1	0.78
Sb_2H	0.2	4.0	1.723	1.878	3.471	1.848	2.32	1.9	1.37
Sb_2Li	–0.9	2.9	2.757	0.412	0.832	2.019	1.05	–6.3	0.64
Sb_2Na	–1.0	2.8	3.078	0.296	0.581	1.963	0.91	–6.6	0.54
Sb_2K	–1.1	2.8	3.660	0.21	0.445	2.119	0.77	–7.36	0.46
Sb_2Rb	–1.1	2.7	3.862	0.19	0.436	2.295	0.70	–7.62	0.44
Sb_2Cs	–1.2	2.6	4.130	0.155	0.369	2.381	0.63	–7.82	0.39
Bi_2F	2.2	5.8	2.180	1.636	1.903	1.163	2.66	10.31	1.28
Bi_2Cl	1.2	4.8						6.41	
Bi_2Br	1.0	4.6	2.757	0.97	2.176	2.243	1.67	5.31	0.98
Bi_2I	0.7	4.3	3.157	0.593	–0.229	–0.386	1.36	4.91	0.77
Bi_2H	0.3	3.9						5.81	
Bi_2Li	–0.8	2.8	2.808	0.388	0.767	1.977	1.00	–2.39	0.62
Bi_2Na	–0.9	2.7	3.126	0.28	0.513	1.832	0.86	–2.69	
Bi_2K	–1.0	2.6	3.656	0.15	0.261	1.740	0.71	–3.45	0.39
Bi_2Rb	–1.0	2.6	3.820	0.165	0.387	2.345	0.68	–3.61	0.41
Bi_2Cs	–1.1	2.5	4.183	0.152	0.347	2.283	0.60	–3.91	0.39
Group 16									
O_2F	0.5	7.5	1.500	3.281	–6.615	–2.016	5.00	3.3	1.81
O_2Cl	–0.5	6.5	1.807	2.347	–1.234	–0.526	3.60	–0.6	1.53
O_2Br	–0.7	6.3	1.857	2.881	2.939	1.020	3.39	–1.7	1.70
O_2I	–1.0	6.0	1.950	2.977	3.909	1.313	3.08	–2.1	1.73
O_2H	–1.4	5.6	1.063	5.111	23.187	4.537	5.27	–1.2	2.26
O_2Li	–2.5	4.5	1.843	1.018	2.211	2.172	2.44	–9.4	1.01
O_2Na	–2.6	4.4	2.105	0.595	1.491	2.506	2.09	–9.7	0.77
O_2K	–2.6	4.4	2.667	0.438	0.869	1.984	1.65	–10.46	0.66
O_2Rb	–2.7	4.3	2.874	0.366	0.505	1.380	1.50	–10.62	0.60
O_2Cs	–2.8	4.2	3.090	0.304	0.334	1.099	1.36	–10.92	0.55

Table S1 (continuation)

S_2F	1.5	6.5	1.817	2.298	1.102	0.480	3.58	7.1	1.52
S_2Cl	0.5	5.5	2.217	1.672	0.134	0.080	2.48	3.2	1.29
S_2Br	0.3	5.3	2.515	1.068	–1.51	–1.414	2.11	2.1	1.03
S_2I	0.0	5.0	2.641	1.136	–2.292	–0.257	1.89	1.7	1.07
S_2H	–0.4	4.6	1.440	2.643	3.407	1.289	3.19	2.6	1.63
S_2Li	–1.5	3.5	2.244	0.708	1.837	2.581	1.56	–5.6	0.84
S_2Na	–1.6	3.4	2.645	0.392	0.803	2.048	1.29	–5.9	0.63
S_2K	–1.6	3.4	3.189	0.285	0.67	2.351	1.07	–6.66	0.53
S_2Rb	–1.7	3.3	3.397	0.248	0.472	1.903	0.97	–6.82	0.50
S_2Cs	–1.8	3.2	3.649	0.209	0.318	1.522	0.88	–7.12	0.46
Se_2F	1.6	6.4	1.965	2.119	2.302	1.086	3.26	3.7	1.46
Se_2Cl	0.6	5.4	2.435				2.22	–0.2	
Se_2Br	0.4	5.2	2.590	1.072	1.287	1.201	2.01	–1.3	1.04
Se_2I	0.1	4.9	2.865	0.962	–0.671	–0.698	1.71	–1.7	0.98
Se_2H	–0.3	4.5	1.577	2.233	2.749	1.231	2.85	–0.8	1.49
Se_2Li	–1.4	3.4	2.241	0.576	1.105	1.918	1.39	–9.0	0.76
Se_2Na	–1.5	3.3	2.809	0.439	0.894	2.036	1.17	–9.3	0.66
Se_2K	–1.5	3.3	3.235	0.259	0.667	2.575	1.02	–10.06	0.51
Se_2Rb	–1.6	3.2	3.408	0.245	0.698	2.849	0.94	–10.22	0.49
Se_2Cs	–1.7	3.1	3.755	0.207	0.468	2.261	0.83	–10.52	0.45
Te_2F	1.9	6.1	2.116	1.743	1.411	0.810	2.88	3.3	1.32
Te_2Cl	0.9	5.1	2.556	1.073	1.141	1.063	2.00	–0.6	1.04
Te_2Br	0.7	4.9	2.765	0.923	1.317	1.427	1.77	–1.7	0.96
Te_2I	0.4	4.6	3.070	0.792	–1.226	–1.548	1.50	–2.1	0.89
Te_2H	0.0	4.2	2.649	0.482	0.912	1.892	1.59	–1.2	0.69
Te_2Li	–1.1	3.1	2.937	0.375	0.815	2.173	1.06	–9.4	0.61
Te_2Na	–1.2	3.0	3.546	0.231	0.482	2.087	0.85	–9.7	0.48
Te_2K	–1.2	3.0	3.745	0.204	0.469	2.299	0.80	–10.46	0.45
Te_2Rb	–1.3	2.9	3.878	0.166	0.489	2.946	0.75	–10.62	0.41
Te_2Cs	–1.4	2.8						–10.92	
Group 17									
F_3	0.0	8.0	1.680	1.480	–5.16	–3.490	4.76	0.0	1.22
F_2Cl	–1.0	7.0	1.773				3.95	–3.9	1.72
F_2Br	–1.2	6.8						–5.0	
F_2I	–1.5	6.5						–5.4	

Table S1 (continuation)

F_2H	–1.9	6.1	1.096	4.642	–1.441	–0.310	5.57	–4.5	2.15
F_2Li	–3.0	5.0	1.737	1.187	2.36	1.990	2.88	–12.7	1.09
F_2Na	–3.1	4.9	2.065	0.787	2.122	2.700	2.37	–13	0.89
F_2K	–3.1	4.9	2.407	0.517	1.52	2.940	2.04	–13.76	0.72
F_2Rb	–3.2	4.8	2.716	0.431	0.658	1.53	1.77	–13.92	0.66
F_2Cs	–3.3	4.7	2.914	0.362	0.445	1.23	1.61	–14.22	0.60
Cl_2F	1.0	7.0	2.036	1.067	–3.924	–3.68	3.44	3.9	1.03
Cl_3	0.0	6.0	2.259	1.605	–1.053	–0.66	2.66	0	1.27
Cl_2Br	–0.2	5.8	2.445	1.403	0.247	0.18	2.37	–1.1	1.18
Cl_2I	–0.5	5.5	2.574	1.328	1.176	0.89	2.14	–1.5	1.15
Cl_2H	–0.9	5.1	1.499	2.522	–1.215	–0.48	3.40	–0.6	1.59
Cl_2Li	–2.0	4.0	2.184	0.753	1.435	1.91	1.83	–8.8	0.87
Cl_2Na	–2.1	3.9	2.526	0.504	1.213	2.41	1.54	–9.1	0.71
Cl_2K	–2.1	3.9	3.049	0.326	0.775	2.38	1.28	–9.86	0.57
Cl_2Rb	–2.2	3.8	3.251	0.289	0.574	1.99	1.17	–10.02	0.54
Cl_2Cs	–2.3	3.7	3.486	0.238	0.380	1.6	1.06	–10.32	0.49
Br_2F	1.2	6.8	2.089	1.679	–1.343	–0.8	3.25	5	1.30
Br_2Cl	0.2	5.8	2.487	1.234	–2.030	–1.65	2.33	1.1	1.11
Br_3	0.0	5.6	2.671	1.200	–0.195	–2.38	2.10	0	1.10
Br_2I	–0.3	5.3	3.371	0.181	–0.430	–2.38	1.57	–0.4	0.43
Br_2H	–0.7	4.9	1.662	1.995	–0.553	–0.28	2.95	0.5	1.41
Br_2Li	–1.8	3.8	2.404	0.540	0.612	1.13	1.58	–7.7	0.73
Br_2Na	–1.9	3.7	2.690	0.453	0.917	2.02	1.38	–8	0.67
Br_2K	–1.9	3.7	3.130	0.283	0.744	2.63	1.18	–8.76	0.53
Br_2Rb	–2.0	3.6	3.300	0.262	0.774	2.95	1.09	–8.92	0.51
Br_2Cs	–2.1	3.5	3.631	0.229	0.516	2.25	0.96	–9.22	0.48
I_2F	1.5	6.5	2.211	1.546	–0.655	–0.42	2.94	5.4	1.24
I_2Cl	0.5	5.5	2.750				2.00	1.5	0.96
I_2Br	0.3	5.3	2.880	0.782	–0.235	–0.3	1.84	0.4	0.88
I_3	0.0	5.0	3.076	0.639	–0.316	–0.49	1.63	0	0.80
I_2H	–0.4	4.6	1.849	1.626	–0.426	–0.26	2.49	0.9	1.28
I_2Li	–1.5	3.5	2.560	0.544	0.967	1.78	1.37	–7.3	0.74
I_2Na	–1.6	3.4	2.967	0.328	0.403	1.23	1.15	–7.6	0.57
I_2K	–1.6	3.4	3.451	0.241	0.499	2.07	0.99	–8.36	0.49

Table S1 (continuation)

I_2Rb	–1.7	3.3	3.648	0.218	0.508	2.33	0.90	–8.52	0.47
I_2Cs	–1.8	3.2	3.770	0.179	0.546	3.05	0.85	–8.82	0.42

* R_0 has been evaluated performing energy scan along symmetric stretching coordinate.
** n.d. = not determined.
*** blank places – for these molecules we met computational problems, as described in the Methods of Calculations section.

Table S2. Calculated geometric, vibrational and vibronic parameters for linear $ABA^{\bullet}$ molecules where A = alkali metal, H or halogen, B = selected d-block element: optimized A–B bond length (R_0/Å), force constant for the symmetric (k_g/mDyne $Å^{-1}$) and antisymmetric stretching (k_u/mDyne $Å^{-1}$), and vibronic stability parameter (**G**/1). Sum and difference of electronegativities between A and B ($EN_A + EN_B$, and Δ EN, respectively) and parameter **f** [arb.u.] are also shown. Molecules are grouped by affiliation of A to a given group or period of the periodic table. Negative values of k_u and **G** indicate imaginary frequency for antisymmetric stretch.

molecule	Δ EN	$EN_A + EN_B$	R_0/Å	k_g/mDyne $Å^{-1}$	k_u/mDyne $Å^{-1}$	**G**/1	**f**/arb.u.
Group 10							
Au2F	1.6	6.4	2.147	1.510	1.374	0.91	2.98
Au2Cl	0.6	5.4	2.475	1.102	1.102	1.00	2.18
Au2Br	0.4	5.2	2.652	0.864	0.941	1.09	1.96
Au2I	0.1	4.9	2.782	0.825	0.987	1.20	1.76
Au2H	–0.3	4.5	*				
Au2Li	–1.4	3.4	2.447	0.480	0.770	1.60	1.39
Au2Na	–1.5	3.3	2.764	0.391	0.726	1.86	1.19
Au2K	–1.6	3.2	3.213	0.276	0.587	2.13	1.00
Au2Rb	–1.6	3.2	3.400	0.231	0.579	2.51	0.94
Au2Cs	–1.7	3.1	3.585	0.206	0.595	2.89	0.86
Ag2F	2.1	5.9	2.175	1.205	1.957	1.62	2.71
Ag2Cl	1.1	4.9	2.528	0.833	1.272	1.53	1.94
Ag2Br	0.9	4.7	2.679	0.757	1.293	1.71	1.75
Ag2I	0.6	4.4	2.830	0.643	0.988	1.54	1.55
Ag2H	0.2	4.0					
Ag2Li	–0.9	2.9	2.545	0.319	0.538	1.69	1.14
Ag2Na	–1.0	2.8	2.826	0.280	0.550	1.97	0.99
Ag2K	–1.1	2.7	3.267	0.193	0.416	2.16	0.83
Ag2Rb	–1.1	2.7	3.453	0.172	0.440	2.56	0.78
Ag2Cs	–1.2	2.6	3.856	0.116	0.176	1.52	0.67
Cu2F	2.1	5.9	1.907	1.688	3.132	1.86	3.09
Cu2Cl	1.1	4.9	2.267	1.066	1.997	1.87	2.16
Cu2Br	0.9	4.7	2.427	0.923	1.727	1.87	1.94
Cu2I	0.6	4.4	2.593	0.789	1.225	1.55	1.70
Cu2H	0.2	4.0	1.563	1.203	1.902	1.58	2.56
Cu2Li	–0.9	2.9	2.492	0.305	0.360	1.18	1.16
Cu2Na	–1.0	2.8	2.699	0.275	0.597	2.17	1.04
Cu2K	–1.1	2.7	3.172	0.176	0.401	2.28	0.85
Cu2Rb	–1.1	2.7	3.354	0.153	0.380	2.48	0.81
Cu2Cs	–1.2	2.6	3.564	0.122	0.286	2.34	0.73

Table S2 (continuation)

Group 4							
Hf2F	2.7	5.3	2.087	1.910	0.880	0.46	2.54
Hf2Cl	1.7	4.3					
Hf2Br	1.5	4.1	2.658	0.910	1.376	1.51	1.54
Hf2I	1.2	3.8	2.803	0.834	1.831	2.20	1.36
Hf2H	0.8	3.4					
Hf2Li	–0.3	2.3	2.721				0.85
Hf2Na	–0.4	2.2	3.447	0.142	0.270	1.90	0.64
Hf2K	–0.5	2.1	4.030	0.074	0.172	2.32	0.52
Hf2Rb	–0.5	2.1	4.220	0.090	0.268	2.98	0.50
Hf2Cs	–0.6	2.0	4.047	0.126	0.258	2.06	0.45
Zr2F	2.6	5.4	2.176	1.606	2.537	1.58	2.48
Zr2Cl	1.6	4.4					
Zr2Br	1.4	4.2	2.681	0.955	2.323	2.43	1.57
Zr2I	1.1	3.9	2.780	1.008	2.670	2.65	1.40
Zr2H	0.7	3.5					
Zr2Li	–0.4	2.4	2.997	0.267	0.598	2.24	0.80
Zr2Na	–0.5	2.3	3.220				0.71
Zr2K	–0.6	2.2	3.774	0.125	0.252	2.02	0.58
Zr2Rb	–0.6	2.2	3.988	0.105	0.247	2.35	0.55
Zr2Cs	–0.7	2.1	4.314	0.098	0.187	1.90	0.49
Ti2F	2.5	5.5					
Ti2Cl	1.5	4.5	2.206	1.612	4.639	2.88	2.04
Ti2Br	1.3	4.3	2.666	0.736	1.091	1.48	1.61
Ti2I	1.0	4.0	2.764	0.678	1.353	2.00	1.45
Ti2H	0.6	3.6					
Ti2Li	–0.5	2.5	3.013	0.240	0.457	1.91	0.83
Ti2Na	–0.6	2.4					
Ti2K	–0.7	2.3	3.599	0.154	0.308	2.01	0.64
Ti2Rb	–0.7	2.3	3.801	0.135	0.254	1.88	0.61
Ti2Cs	–0.8	2.2					
Period VI							
Pt2F	1.8	6.2	2.063	1.732	2.321	1.34	3.01
Pt2Cl	0.8	5.2	2.298				
Pt2Br	0.6	5.0	2.570	0.944	1.905	2.02	1.95
Pt2I	0.3	4.7	2.750	0.958	1.335	1.39	1.71
Pt2H	–0.1	4.3					
Pt2Li	–1.2	3.2	2.418	0.523	0.926	1.77	1.32
Pt2Na	–1.3	3.1	2.774	0.391	0.724	1.85	1.12
Pt2K	–1.4	3.0	3.207	0.270	0.595	2.20	0.94
Pt2Rb	–1.4	3.0	3.386	0.227	0.603	2.66	0.89
Pt2Cs	–1.5	2.9	3.559	0.211	0.659	3.13	0.81
Ir2F	1.8	6.2					
Ir2Cl	0.8	5.2					
Ir2Br	0.6	5.0	2.518	1.331	3.190	2.40	1.99
Ir2I	0.3	4.7	2.763				1.70
Ir2H	–0.1	4.3					

Table S2 (continuation)

Ir2Li	–1.2	3.2	2.529	–0.488	–0.750	–1.54	1.27
Ir2Na	–1.3	3.1	2.842				1.09
Ir2K	–1.4	3.0	3.270	0.243	0.486	2.00	0.92
Ir2Rb	–1.4	3.0	3.461	0.210	0.491	2.33	0.87
Ir2Cs	–1.5	2.9	3.652	0.167	0.444	2.66	0.79
Os2F	1.8	6.2					
Os2Cl	0.8	5.2					
Os2Br	0.6	5.0	2.578				1.94
Os2I	0.3	4.7	2.802	0.882	0.114	0.13	1.68
Os2H	–0.1	4.3					
Os2Li	–1.2	3.2	2.629	0.422	0.555	1.32	1.22
Os2Na	–1.3	3.1	2.922	0.343	0.562	1.64	1.06
Os2K	–1.4	3.0	3.288				0.91
Os2Rb	–1.4	3.0	3.470	0.210	0.541	2.57	0.86
Os2Cs	–1.5	2.9	3.799	0.155	0.332	2.15	0.76
Period V							
Pd2F	1.8	6.2	2.103	1.422	2.477	1.74	2.95
Pd2Cl	0.8	5.2					
Pd2Br	0.6	5.0	2.564	0.931	2.376	2.55	2.42
Pd2I	0.3	4.7	2.693	0.861	2.334	2.71	1.75
Pd2H	–0.1	4.3					
Pd2Li	–1.2	3.2	2.345	0.458	0.834	1.82	1.36
Pd2Na	–1.3	3.1	2.697	0.361	0.819	2.27	1.15
Pd2K	–1.4	3.0	3.054	0.213	0.519	2.44	0.98
Pd2Rb	–1.4	3.0	3.210	0.208	0.642	3.08	0.93
Pd2Cs	–1.5	2.9	3.331	0.181	0.578	3.20	0.87
Rh2F	1.8	6.2	2.092	1.449	2.688	1.86	2.96
Rh2Cl	0.8	5.2					
Rh2Br	0.6	5.0	2.568	0.960	2.554	2.66	1.95
Rh2I	0.3	4.7	2.645				1.78
Rh2H	–0.1	4.3					
Rh2Li	–1.2	3.2	2.359				1.36
Rh2Na	–1.3	3.1	2.738	0.332	0.787	2.37	1.13
Rh2K	–1.4	3.0	3.134	0.165	0.368	2.23	0.96
Rh2Rb	–1.4	3.0	3.244	0.175	0.572	3.27	0.92
Rh2Cs	–1.5	2.9	3.683	0.127	0.241	1.89	0.79
Ru2F	1.8	6.2					
Ru2Cl	0.8	5.2					
Ru2Br	0.6	5.0	2.607	0.740	2.263	3.06	1.92
Ru2I	0.3	4.7	2.735	0.621	2.304	3.71	1.72
Ru2H	–0.1	4.3					
Ru2Li	–1.2	3.2	2.550	0.342	0.409	1.20	1.25
Ru2Na	–1.3	3.1	2.834	0.297	0.662	2.23	1.09
Ru2K	–1.4	3.0	3.257	0.199	0.504	2.53	0.92
Ru2Rb	–1.4	3.0	3.446	0.171	0.511	2.99	0.87
Ru2Cs	–1.5	2.9	3.680	0.125	0.372	2.98	0.79

*blank places – for these molecules we met computational problems, as described in the Methods of Calculations section.